UNLV | UNIVERSITY LIBRARIES

Transmutation Sciences Materials (TRP) | Transmutation Research Program Projects

8-30-2003

Modeling Corrosion in Oxygen Controlled LBE Systems with Coupling of Chemical Kinetics and Hydrodynamics-Task V: Annual Report -Phase II 09/01/2002-08/30/2003

Samir Moujaes
University of Nevada, Las Vegas, samir@me.unlv.edu

Yitung Chen
University of Nevada, Las Vegas, yitung.chen@unlv.edu

Follow this and additional works at: https://digitalscholarship.unlv.edu/hrc_trp_sciences_materials

 Part of the Materials Chemistry Commons, Metallurgy Commons, Nuclear Engineering Commons, and the Oil, Gas, and Energy Commons

Repository Citation

Moujaes, S., Chen, Y. (2003). Modeling Corrosion in Oxygen Controlled LBE Systems with Coupling of Chemical Kinetics and Hydrodynamics-Task V: Annual Report -Phase II 09/01/2002-08/30/2003. 1-37.
Available at: https://digitalscholarship.unlv.edu/hrc_trp_sciences_materials/72

This Annual Report is protected by copyright and/or related rights. It has been brought to you by Digital Scholarship@UNLV with permission from the rights-holder(s). You are free to use this Annual Report in any way that is permitted by the copyright and related rights legislation that applies to your use. For other uses you need to obtain permission from the rights-holder(s) directly, unless additional rights are indicated by a Creative Commons license in the record and/or on the work itself.

This Annual Report has been accepted for inclusion in Transmutation Sciences Materials (TRP) by an authorized administrator of Digital Scholarship@UNLV. For more information, please contact digitalscholarship@unlv.edu.

Modeling Corrosion in Oxygen Controlled LBE Systems with Coupling of Chemical Kinetics and Hydrodynamics-Task V

Annual Report -Phase II
09/01/2002-08/30/2003
UNLV-TRP University Participation Program

Principle Investigator: Samir Moujaes
Co-Principle Investigator: Yitung Chen

Purpose and Problem Statement

The Lead-Bismuth eutectic (LBE) has been determined from previous experimental studies by the Russians and the European scientific community to be a potential material that can be used as a spallation target and coolant for the TRP proposed application. Properly controlling the oxygen content in LBE can drastically reduce the LBE corrosion to structural steels. However, existing knowledge of material corrosion performance was obtained from point-wise testing with only very sparse experimental data. Scientists have noticed that the concentration of oxygen dissolved in the liquid alloy could control the corrosion rate of steels exposed to Pb or Pb-Bi. At high oxygen concentration, an oxide layer could be formed on the steel surface (lead oxides are less stable than iron oxide), which protects it from corrosion. At low oxygen concentration, there is no oxidation and corrosion occurs by dissolution of the steel components in the liquid metal. The surface of the oxide layer in contact with the bulk flow of liquid metal may also be eroded under a high fluid velocity. Then the surface of the metal will no longer be protected because a porous oxide layer will be formed.

The first subtask of this project involves using a CFD code (3-D simulation) such as STAR-CD to obtain averaged values of stream wise velocity, temperature, oxygen and corrosion product concentrations at a location deemed close to the walls of the LBE loop at more than one axial location along it. The oxygen and corrosion product inside the test loop will be simulated to participate in chemical reactions with the eutectic fluid as it diffuses through towards the walls. Details of the geometry of these loops will be obtained from scientists at LANL. These values will act as a set of starting boundary conditions to the second task.

The second subtask and the more important objective of this project is to use the information supplied by the first task as boundary conditions for the kinetic modeling of the corrosion process at the internal walls of the test loop. The outcome of the modeling will be fed back to the first subtask, and the steady state corrosion/precipitation in an oxygen controlled LBE system will be investigated through iterations. The information is hoped to shed some light on the likely locations for corrosion and precipitation along the axial length of parts of the test loop.

Personnel

Principle Investigator:

- Dr. Samir Moujaes (Mechanical Engineering)

Co-Principle Investigator:

- Dr. Yitung Chen (Mechanical Engineering)

Students:

- Mr. Kanthi Kiran Dasika, M.S. Graduate Student, (Mechanical Engineering)
- Mr. Chao Wu, M.S. Graduate Student, (Mechanical Engineering)

National Laboratory Collaborator:

- Dr. Ning Li, Project Leader, Lead-Bismuth Material Test Loop, LANL
- Dr. Jinsuo Zhang, Post Doctoral Candidate, LANL

Technical progress:

Introduction:

Liquid lead-bismuth eutectic is considered as a prototype target and coolant for the Transmutation Research Project (TRP). It is an alloy of 45% lead and 55% bismuth with the melting temperature of 123.5^{o}C and boiling temperature of 1670^{o}C. Using liquid lead-bismuth eutectic (LBE) as coolant in nuclear systems has been studied for more than 50 years. LBE has many unique nuclear, thermo physical and chemical attributes that are attractive for nuclear coolant applications. This liquid's relatively low melting point and high boiling point in addition to good heat transfer properties make it a very good candidate for coolant. In addition, lead and bismuth can produce copious spallation neutrons when bombarded with energetic protons. This makes LBE one of the top candidates for a high-power spallation target in an Accelerator-driven Transmutation of Waste (ATW) system. Besides, the use of heavy liquid metal like LBE as a coolant for fast reactors offers several safety and economic advantages. These arise from the following basic material characteristics: chemical inertness with air and water, high atomic number, high boiling temperature and low vapor pressure at operating temperatures. Specifically, heavy-metal coolants do not react energetically with air and water; therefore, coolant fires are not possible and an intermediate heat transport loop is unnecessary. Also, the hard neutron spectrum achievable with these coolants enables the design of cores with minimal neutronic reactivity swing, small control requirements and long neutronic life time. The significantly lower reactivity associated with hypothetical voiding of the coolant, as compared to sodium, makes it possible to design lead or lead-bismuth-cooled cores with a negative coolant void coefficient, there by eliminating the possibility of severe accidents from consideration. Finally, lead or lead-bismuth coolants provide better shielding against gamma-rays and energetic neutrons, so that less shielding structures are needed. Liquid spallation source also eliminates some of the structural damage problems associated with the targets. Combining the target and coolant roles in one material allows for a simple target design.

One of the critical obstacles to the wide use of LBE as a nuclear coolant, though, is corrosion. The corrosion processes need to be controlled and reduced or they lead to severe safety problems. Unprotected steel undergoes severe attack by liquid lead and lead-bismuth alloy by dissolution of its components in the liquid metal. During the last years, not much was known about possibilities to improve the compatibility of steel with liquid Pb and Pb/Bi. Some compatibility tests with ferritic steels were reported which revealed corrosion attack can be

minimized if an oxide layer exists on the steel surface. Scientists at IPPE, Obninsk, Russia, discovered that if an oxide film is allowed to form on the steel surface it prevents corrosion. This protective film consists mostly of steel components' oxides and it is based on Fe_3O_4. Formation and longevity of this protective film depends on oxygen concentration on the liquid metal. In order to use liquid lead-bismuth in AAA facility, we need to know how to control corrosion of structural materials.

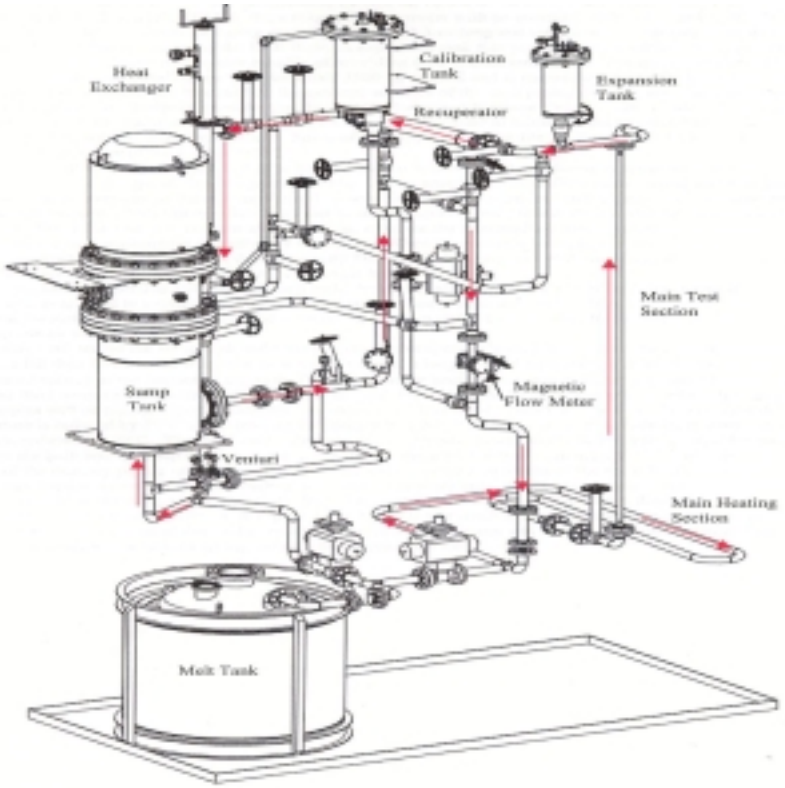

Figure – 1: Materials Test Loop

The active oxygen control technique exploits the fact that lead and bismuth are chemically less active than the major components of steels, such as Fe, Ni, and Cr. By carefully controlling the oxygen concentration in LBE, it is possible to maintain an iron and chrome oxide based film on the surfaces of structural steels, while keeping lead and bismuth from excessive oxidation that can lead to precipitation contamination. The oxide film, especially the compact portion rich in Cr, effectively separates the substrates from LBE. Once this oxide film is formed on the structure surface, the direct dissolution of structural materials becomes negligible because the diffusion rates of the alloying components are very small in the oxides. In this circumstance, the only effective means of transferring structural materials into LBE is through the reduction of the oxide film at the interface of the film and LBE. The Los Alamos National Laboratory's Accelerator-driven Transmutation of Waste (ATW) applications and the Department of Energy's TRP program have invested in developing LBE technology from spallation target and nuclear coolant applications since 1997. A Materials Test Loop (MTL) has been set up in Los Alamos. The MTL is a facility designed to test the safe operation of a medium-size, forced circulation LBE system with representative thermal hydraulic conditions (as spallation target and/or transmutation blanket systems), to perform corrosion tests, and to develop candidate materials

with oxygen control (and related probes and control systems). Figure-1 shows the skeleton representation of the MTL.

It has been well known that fluid flow influences corrosion in many ways, including the increase of the diffusion of reactant species and the transport of potentially protective corrosion product forming ions away from surface. In the mass transfer controlled regime, the corrosion rate is determined by the mass transfer coefficient and the gradient between the corrosion product concentration at the solid-liquid interface and the concentration in the bulk flow. Corrosion rate is typically a function of local temperature and flow velocity. However, corrosion and precipitation rates and distributions can depend strongly on the global temperature distribution, limiting the applicability of many corrosion models.

The present study involves the estimation of corrosion in the liquid metal, by imposing an analytically developed concentration expression on the wall surfaces and thus benchmarking the CFD tool and performing a series of parametric studies on the loop model. The concentration and temperature diffusions due to different flow regimes have been studied. Regions of maximal corrosion and precipitation have been deduced from the simulations and the results have been compared with the analytical models. STAR-CD has been chosen as the CFD code for this purpose.

Numerical Simulation Technique:

The STAR-CD computer simulation code was chosen for the purpose of performing the Computational Fluid Dynamics (CFD) calculations for this project. STAR-CD is a commercially available code that is offered by ADAPCO Co. out of New York State. The code is a transient multidimensional simulator for Thermal hydraulics and chemical reactions occurring in the fluid flow itself.

STAR-CD is a general-purpose code that solves numerically a set of differential equations that describe the following conservation laws: mass conservation, momentum, energy and chemical species. The following equations are solved by this code:

Continuity Equation:

$$u_{i,i} = 0 \tag{1}$$

Momentum Equation:

$$\rho_0 [\frac{\partial u_i}{\partial t} + u_i u_{i,j}] = - P_{,i} + [\mu (u_{i,j} + u_{j,i})]_{,j} \tag{2}$$

Energy Equation:

$$\rho_o C_p (\frac{\partial T}{\partial t} + u_i T_{,i}) = (K * T_{,i})_{,i} + \mu \Phi \tag{3}$$

Species Transport:

$$\rho (\frac{\partial C_n}{\partial t} + u_i C_{n,i}) = (\rho \alpha_n C_{n,i}) + q_{c_n} + R_n \tag{4}$$

Due to the Re number estimate for flow in a LBE loop a turbulent flow model should be used as a constitutive model for the momentum transport. It was decided that a k-ε model is to be

used to account for that behavior. The model consists of adding two more non-linear (transport equations) partial differential equations to each unknown nodal location. The k denoted the turbulent kinetic energy $\overline{u_i u_i}$ and the ε is the viscous dissipation rate of the turbulent kinetic energy $\upsilon \overline{u_{i,j} u_{i,j}}$. The resulting equations are:

k – transport equation:

$$\rho_o\left(\frac{\partial k}{\partial t} + u_i u_{i,j}\right) = \left(\mu_o + \frac{\mu_t}{\sigma_k} k_{,j}\right)_{,j} + \mu_t \Phi + \mu_t g_i \left(\frac{\beta_T}{\sigma_t} T_{,j}\right) - \rho_o \varepsilon \qquad (5)$$

ε – transport equation:

$$\rho_o\left(\frac{\partial \varepsilon}{\partial t} + u_j \varepsilon_j\right) = \left(\mu_o + \frac{\mu_t}{\sigma_k}\right)_{,j} + c_1 \frac{\varepsilon}{k} \mu_t \Phi + c_1 (1 - c_3) \frac{\varepsilon}{k} g_i - \rho_o c_2 \frac{\varepsilon^2}{k} \qquad (6)$$

Overall Corrosion Modeling:

Benchmark Study:

This section presents the various models that have been created and used for fluid flow simulation and corrosion estimation in the Materials Test Loop. The benchmark study basically talks about comparing the simulation results with the analytical results and benchmarking the CFD package. The benchmark study also verifies the dependency of the grid distribution with the outcome of the results i.e., to check that the results are grid independent. Primarily, three different models have been considered to replicate the MTL that have been named as

1. Straight Pipe Model
2. Toroidal Loop Model
3. Rectangular Loop Model

Before going into the details of describing each model, an outline of the different assumptions made, need to be stated. The assumptions specified here are for all the models.

For all the models that have been considered, the length of the MTL is assumed to be 5m. This is primarily because of the difficulties in running the large length to diameter ratio models using STAR-CD. The 5m-loop length assumption seems to be reasonable, due to the fact that the imposed conditions on the model are similar to the original loop. The overall diameter of the loop is assumed to be uniform and has been taken as 1 inch or 0.025m. The wall temperatures are assumed to be varying from 623^{o}K to 823^{o}K and the imposed wall concentration is a function of temperature, given by equation 7.

$$c_{Fe} = c_{surf} = \min\left(c_o^{-4/3} * 10^{11.35 - (12844/T)}, 10^{6.01 - (4380/T)}\right) \qquad (7)$$

It is assumed that the flow is incompressible, and that the variation of physical properties of the LBE with the variation of temperature in the given range of 623^{o}K to 823^{o}K is negligible. The table below elaborates on the properties of LBE used for the analysis.

Properties	Density (kg/m^3)	Molecular Viscosity (N/ m^2)	Specific Heat (C J/KgK)	Conductivity (K W/mK)
	1.018E+04	1.018E-03	1.465E+02	1.419E+01

Table – 1: Properties of Lead Bismuth Eutectic

The diffusivity of the iron into the LBE is taken to be 1.0E-08 m^2/s for the all the benchmark study models. The Schmidt number is the ratio of the diffusivity and molecular viscosity, which comes out to be 10 for the case when diffusivity is 1.0E-08 m^2/s.

Figure 2 shows the imposed wall temperature and concentration profiles along the loop length used for the benchmark study and few cases of the parametric study. As can be seen from the figure, the wall temperature varies linearly in the recuperator, heater and heat exchanger zones. The loop length in the figure has been non-dimensionalized. The units of the wall temperature and wall concentration are in Kelvin and parts per million (ppm) respectively.

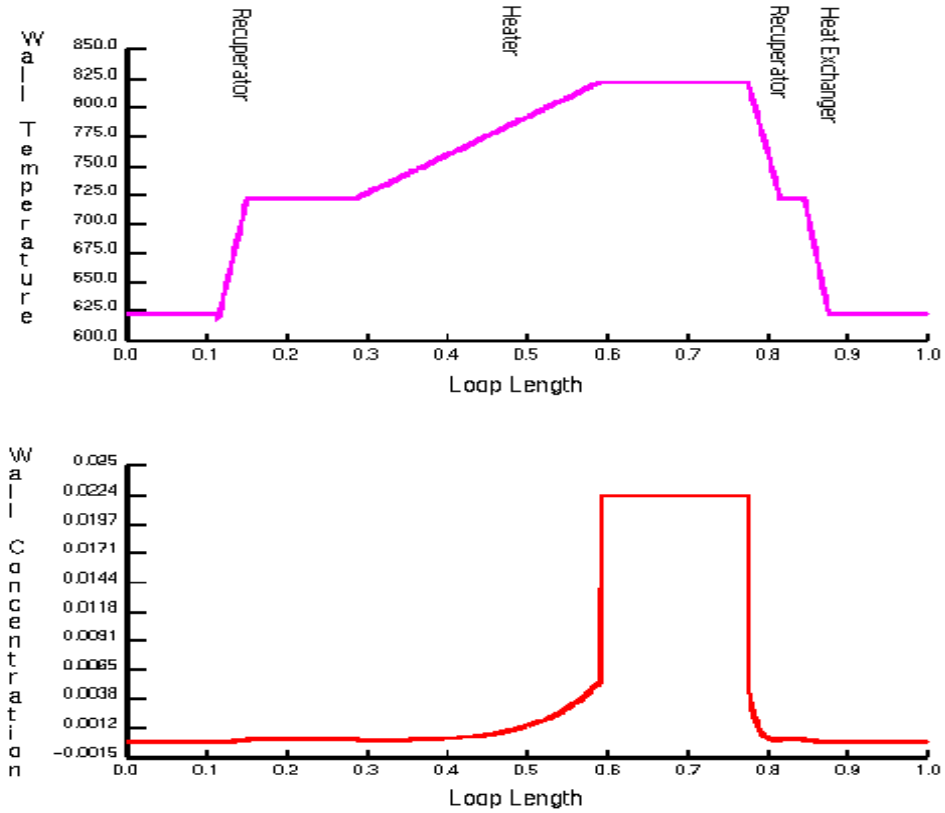

Figure – 2: Imposed wall temperature and concentration for the MTL

Also, for the straight pipe and toroidal loop models, the simulations are carried out in 2D, where as for the rectangular loop model, the simulations are carried out in 3D, due to the complexity of the geometry. For the rectangular loop model, a series of parametric studies have been worked out and the simulations included the modeling in both laminar and turbulent regimes. The straight pipe model included the benchmark study in the turbulent regime; and, for

the toroidal loop model, the simulations did not include the parametric study, nor did they have the studies in the laminar regime, the reasons of which will be detailed in the subsequent discussion. The following subheadings discuss each of the above-mentioned models in detail.

Straight Pipe Model:

For this model, the MTL is considered as a straight pipe with a single inlet and single outlet. The model has been assumed as an open pipe, where the flow coming out from the outlet has not been fed again into the pipe as inlet for simulating the loop. This prototype has a uniform radius of 0.025m and a length of 5m and the LBE enters the pipe with an initial temperature of 623K and an initial concentration of 0ppm, and as specified before, the model has been run as a 2D model. Studies included the flow modeling in turbulent regime for the benchmark study.

Figure 3 shows the skeleton of the straight pipe model considered for the flow analysis. The picture has been zoomed into the inlet region for a clear view of the prototype. As can be seen from the figure, the region near the wall has been refined to a fair degree. The refinement is necessary to capture the mass diffusion of the species from the wall into the fluid, as the diffusion is very prominent in near the wall region than in the bulk of the fluid.

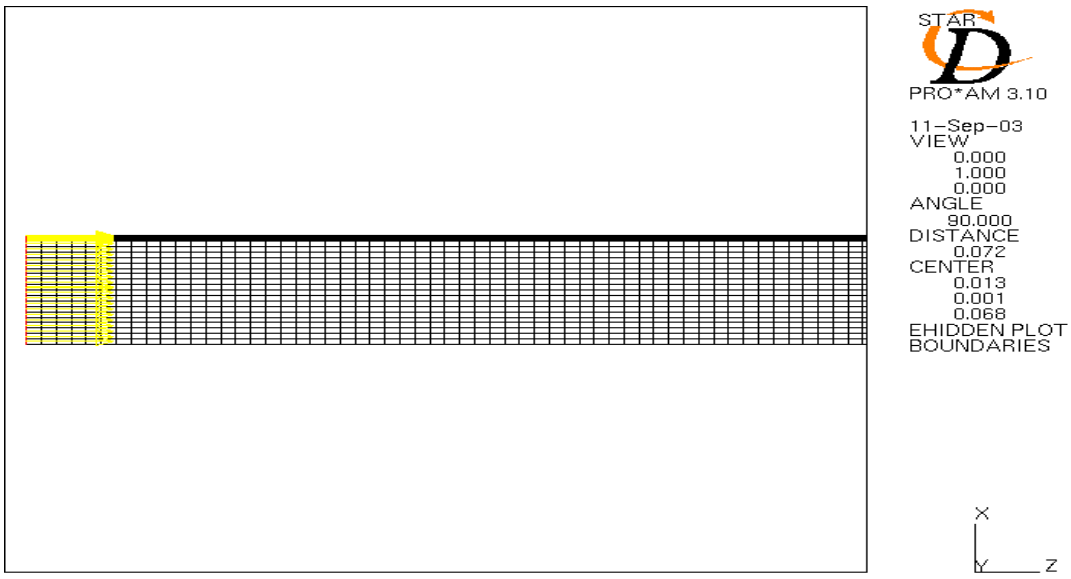

Figure – 3: Straight pipe model

For performing the benchmark study for this model, the simulation has been run with the above-specified assumptions. Care has been taken that the boundary conditions match exactly with the conditions in the DELTA loop and the analytical calculations. The imposed inlet velocity is 0.4m/s, which result in the Reynolds number 200,000. The wall temperature and concentrations have been set according to figure 2.

Figure 4 shows the velocity profiles in the straight pipe model. As expected, the velocity profile in the turbulent flow is flat in the bulk region.

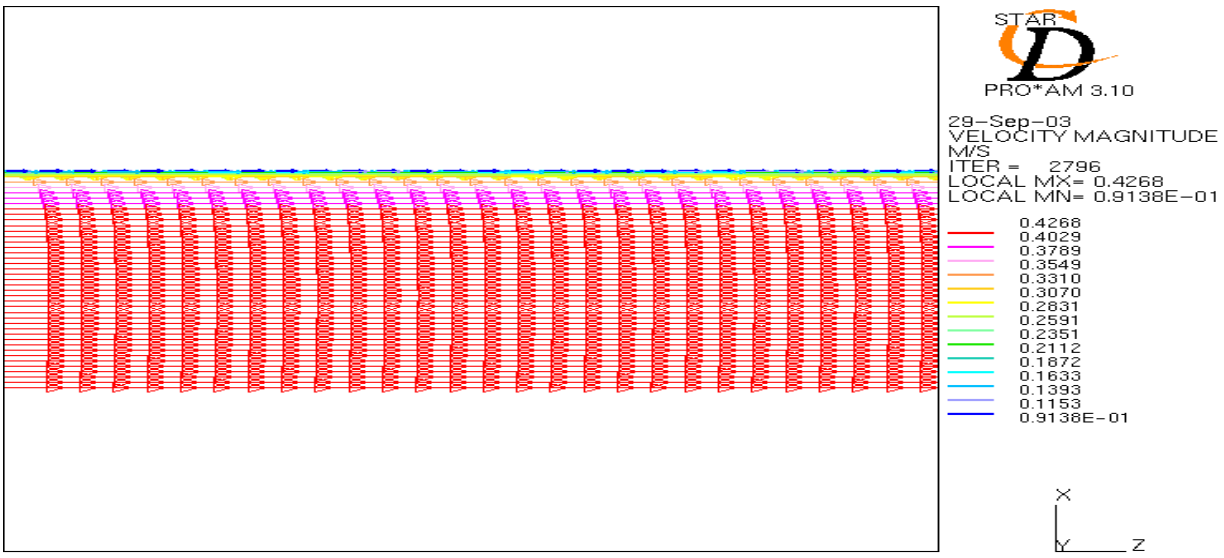

Figure – 4: Velocity Profile for the straight pipe model for a turbulent flow

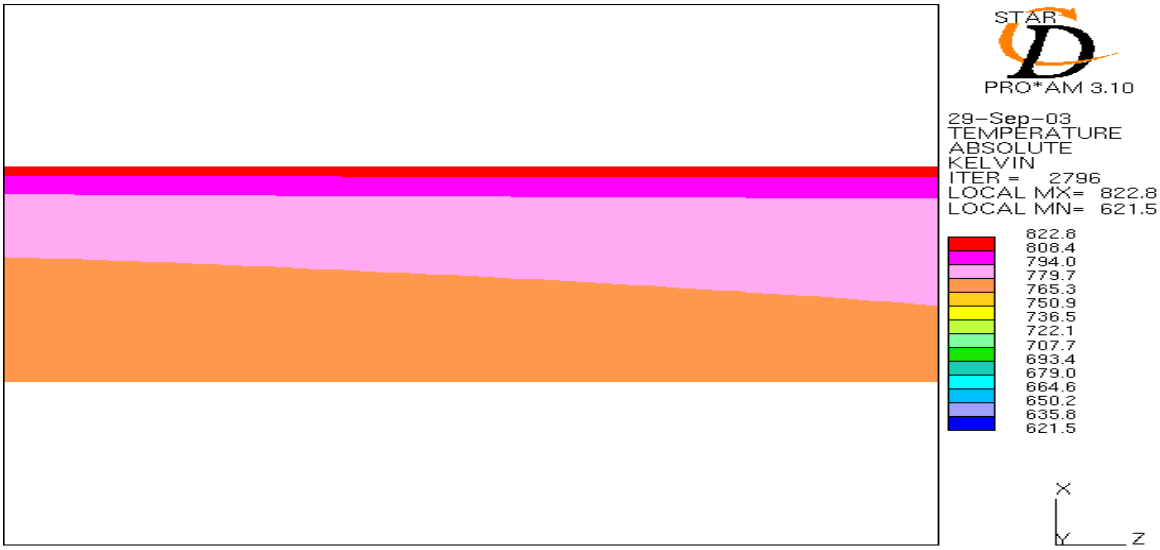

Figure – 5: Temperature profile for the turbulent flow at the recuperator zone of MTL

Figure 5 shows the temperature profile for the model at the test section and figure 6 shows the concentration profile of the straight pipe model at the same section. The diffusion of temperature and concentration could be visualized clearly from both the figures. Since the flow is turbulent and the diffusivity is low, the concentration of the fluid in the bulk is zero equal to the inlet concentration. The diffusion can only be seen in the near wall region.

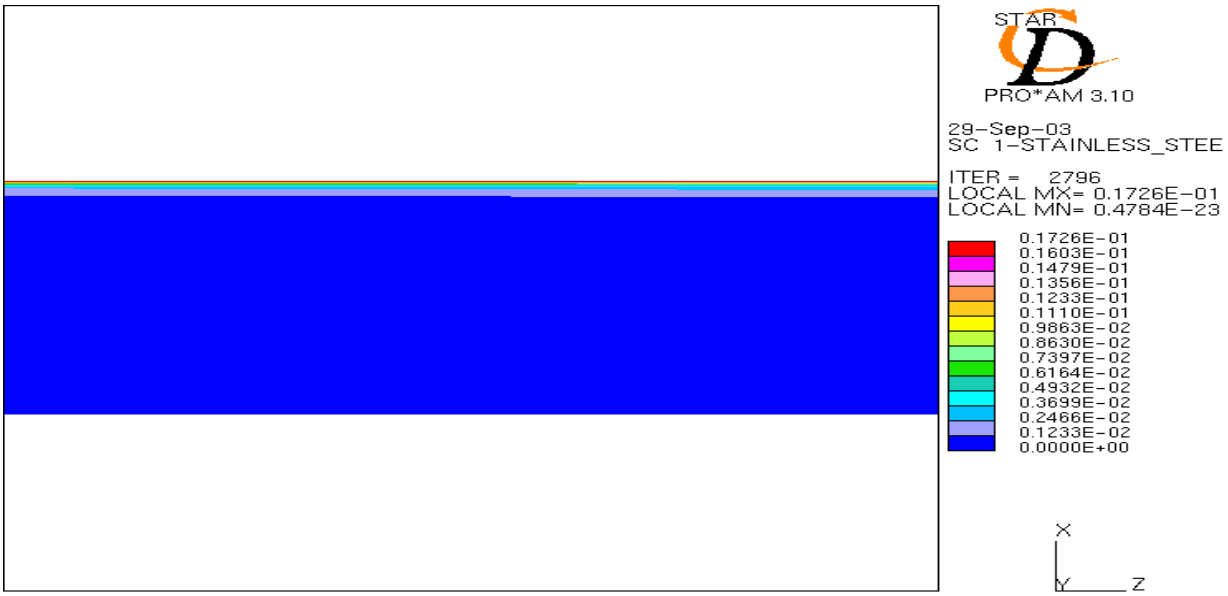

Figure – 6: Concentration profile for the turbulent flow at the main heating section of MTL

The obtained results are then compared to the analytical results. The main parameter of comparison is the corrosion/precipitation rate, which is proportional to the concentration flux. Figure 7 shows the plot of the corrosion rate Vs loop length for the analytical model. As can be seen from the figure 7, the plot shows the corrosion or precipitation variation for both the straight pipe case and the straight loop case at three different temperature variations along the loop length. For the current benchmark study for this model, the simulation results have been compared with the straight pipe with a temperature variation of 200^{o}C.

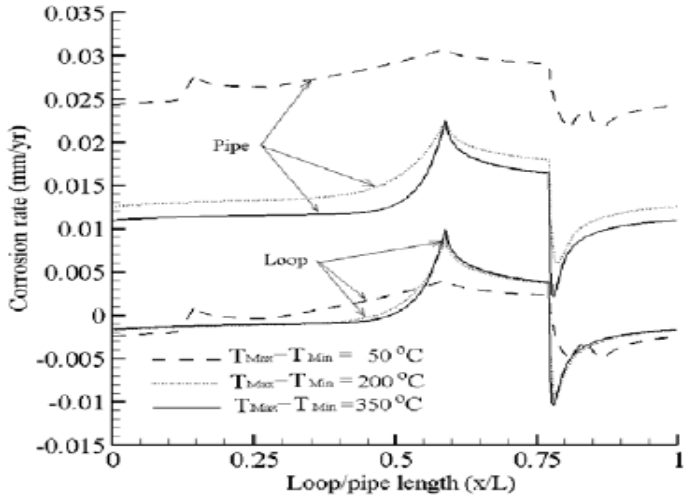

Figure – 7: Corrosion/precipitation rate from the analytical models

Figure 8 shows the graph of concentration flux Vs loop length for the simulated model. As can be seen from figure 8, three different graphs one overlaid on the other have been plotted. All the three graphs represent the same parameter, i.e. the concentration flux, but with three

different mesh structures. The three different mesh structures have been considered to check the dependence of grid structure on the results. The different mesh sizes, in the 'r' and 'z' directions, taken for the checking the grid independency are,

1. 40 X 1000
2. 60 X 1000
3. 80 X 1000

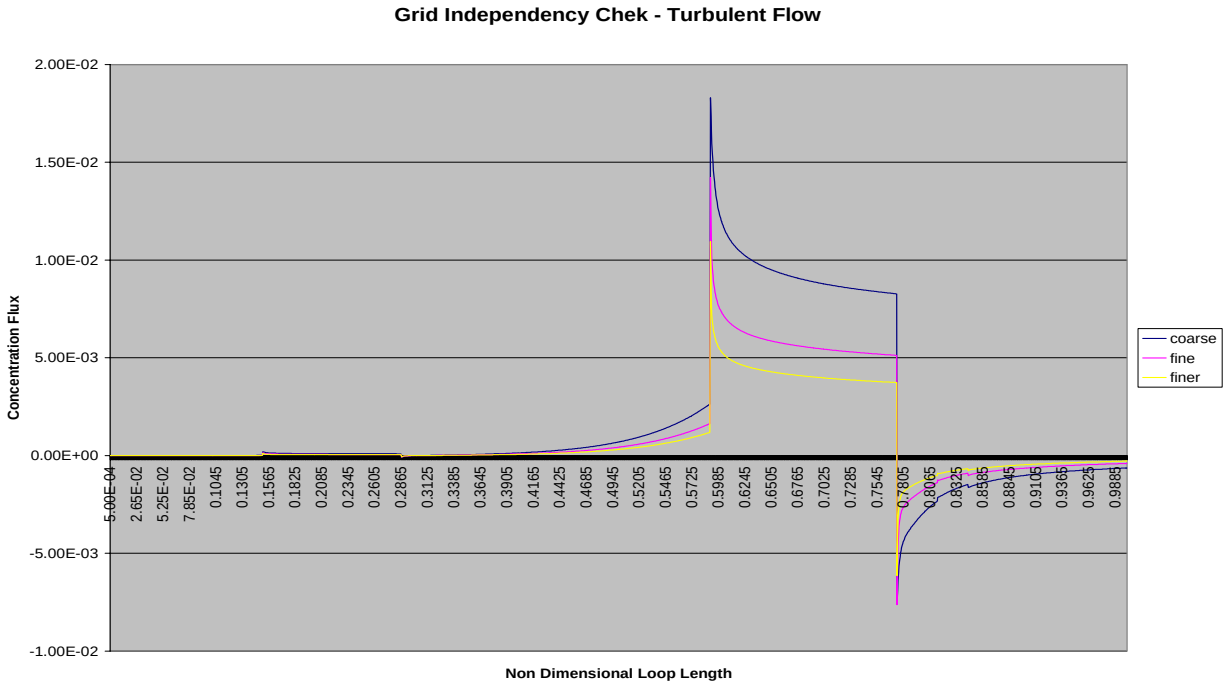

Figure – 8: Corrosion / Precipitation rate and Grid Independency Check for a Straight pipe model

Here, the coarse, fine and finer labels refer to the mesh structures 1, 2 and 3 above. It can be observed that the results are not completely grid independent for this case. A considerable amount of variation can be seen between the three graphs. But the 'fine' and 'finer' mesh seems to be closer to each other than the 'coarse' mesh. Hence the results from the coarse mesh have been considered for comparison with the analytical results.

As can be seen, the results from the analytical and simulated models are fairly close. Hence it has been concluded that the selected CFD package solves the purpose of simulating the MTL with fairly decent results. The benchmarking process, though, was not stopped at this point, since the loop conditions are not involved for this case. The following discussion elaborates on benchmarking the STAR-CD package.

Toroidal Loop Model

The straight pipe model described above cannot be considered as a replica of the MTL, the primary reason being that the above model is an open pipe, where as the MTL is a closed loop. Though the straight pipe model can predict the regions of maximal corrosion and precipitation accurately, the actual values are different from the values obtained from the runs, due to the absence of the closed loop condition. The studies for the straight pipe model have

basically been carried out to compare the results with the analytical models and to check the capabilities of the CFD code.

The analytical models that have been developed previously, assumed the MTL as a straight loop. The loop situation is simulated by feeding the outlet data from one run as an inlet data for the subsequent run. Attempts were made to carry out the simulations in the same way. But due to some technical difficulties, the runs could not be operated. The main difficulty in creating a straight loop model in STAR-CD is that the inlet position for a run should be exactly at the same geometrical position as the outlet position of the previous run, to feed the data from the outlet from one run, as an inlet for the successive run. As can be envisaged, this results in creation of a large number of geometric models for performing a single converged run. This ruled out the creation of a closed straight loop model.

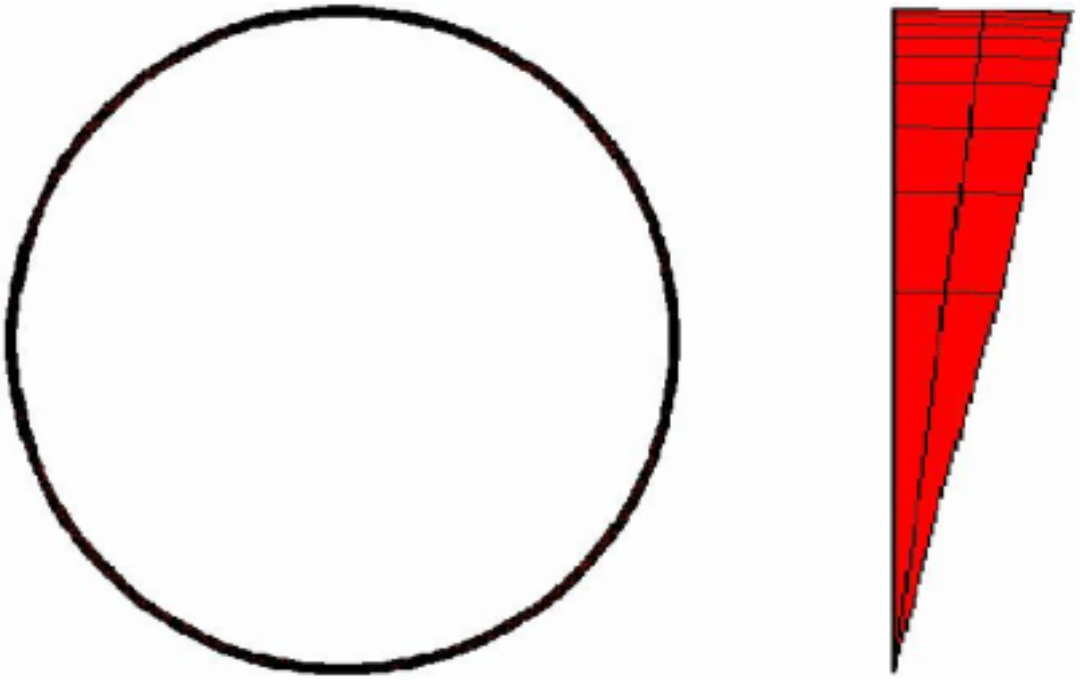

Figure – 9: Toroidal Loop Model

The next closest assumption for the straight loop model is a toroidal geometry with a large radius of curvature. This almost replicates the closed straight loop model, as the secondary flows are negligible in donut shaped geometry with a large radius of curvature. Figure 9 shows the toroidal loop geometry considered for modeling the MTL. As indicated before, the geometry is considered as 2D, due to the absence of complicated secondary flows.

To replicate the pump, a momentum source term has been incorporated in the model. The momentum source, primarily, acts as a source of flow and continuously pumps the fluid in the model at a uniform velocity at the specified location. In the numerical terms, the fluid is pumped at the specified location, after each iteration. In the process, it transfers all the output results, except the velocity, from one iteration, as input for the next iteration. Hence, the momentum is not conserved in this process. But this could be neglected as the elements of primary concern are the temperature and concentration.

Boundary conditions, similar to the straight pipe model, have been applied for this model, excepting for the inlet velocity, which is 6 m/s with a Reynolds number of 2000000. One of the main difficulties faced, though, by using the toroidal loop model is, a linearly variant temperature profile could not be imposed on the walls. For this reason, the regions, where there was a linear increment or decrement of temperature and concentration on the walls, step increment and step decrement of these variables had to be imposed.

The model has been run in the turbulent regime with the mesh distribution of 10 X 2 X 1000. The two divisions in the theta direction have been used for the ease in applying the boundary conditions. Figures 10, 11 & 12 show the velocity, temperature and concentration profiles respectively at the main heating section of the MTL, assuming the geometry of the MTL to be a toroid.

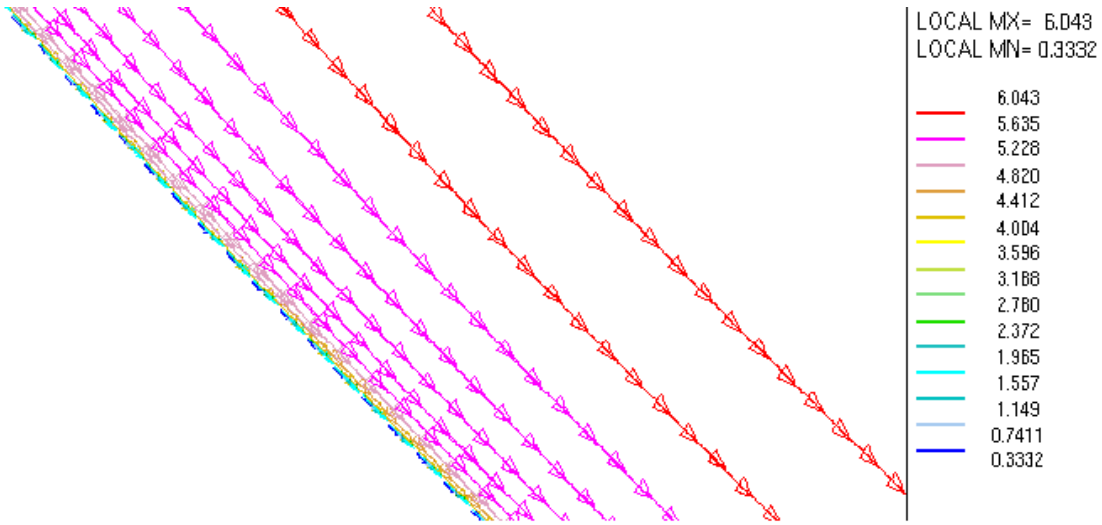

Figure 10: Velocity profile due to turbulent flow at the main test section in the closed toroidal loop model

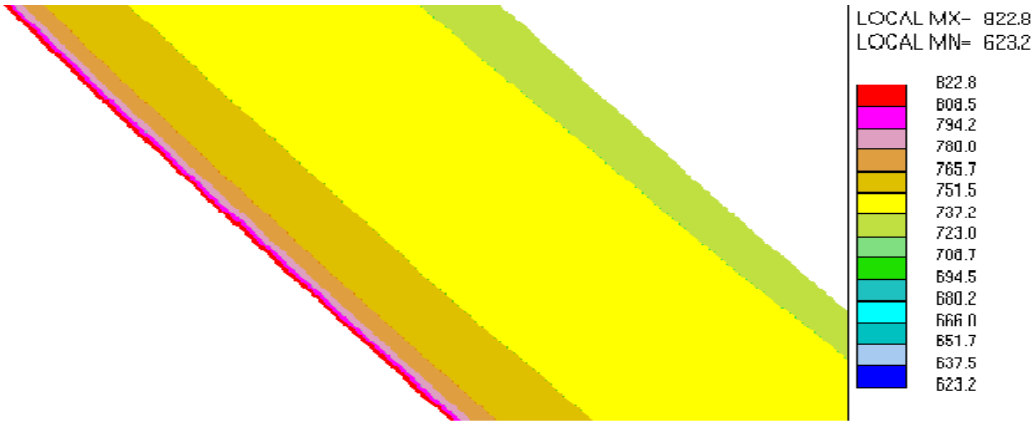

Figure 11: Temperature profile due to the turbulent flow at the main test section in the closed toroidal loop model

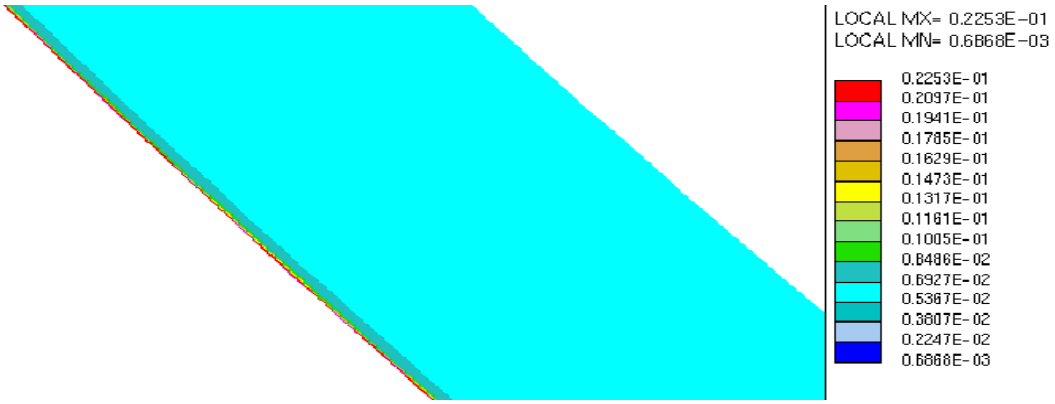

Figure 12: Concentration profile due to the turbulent flow at the main test section in the closed toroidal loop model

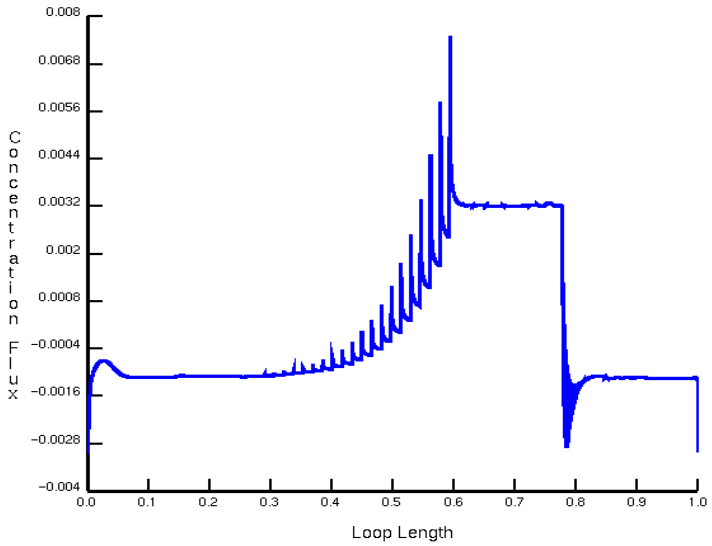

Figure 13: Corrosion/precipitation rate for the closed toroidal loop model

Figure 13 shows the plot of the concentration flux drawn against the loop length for a toroidal loop model. This has been compared to the straight loop model with a temperature variation of 200C in figure 7. The effect of the approximation of a step input is clearly visible as the rise of the concentration flux is not uniform. Though the maximal corrosion and precipitation regions seemed to be in good agreement with the analytical results, as can be seen from the figure, the graphs showed a few peaks and valleys in the areas where step increment/decrement was approximated for linear increment/decrement. The peculiar behavior of a sudden rise and fall at the starting and the end of the loop is due to the inclusion of the momentum source term to simulate the pump.

Rectangular Loop Model

As explained before, the assumption of the MTL as a toroidal loop did not yield good results, due to the step input approximation for wall temperature. The next closest assumption for the MTL is a closed rectangular loop model with a circular cross section. Because of the non-

symmetry, and due to the active participation of the secondary flows due to the elbows present in the rectangular loop model, the geometry can no longer be solved as 2D problem. Hence a 3D model, as shown in the figure 14 has been considered for this case. The region near the wall has been greatly refined for the reasons explained before.

The initial and boundary conditions for this model are same as the ones for the straight pipe model, excepting for the momentum source term. Momentum source has been applied to replicate the pump. The wall temperature and concentration profiles were applied according to figure 2.

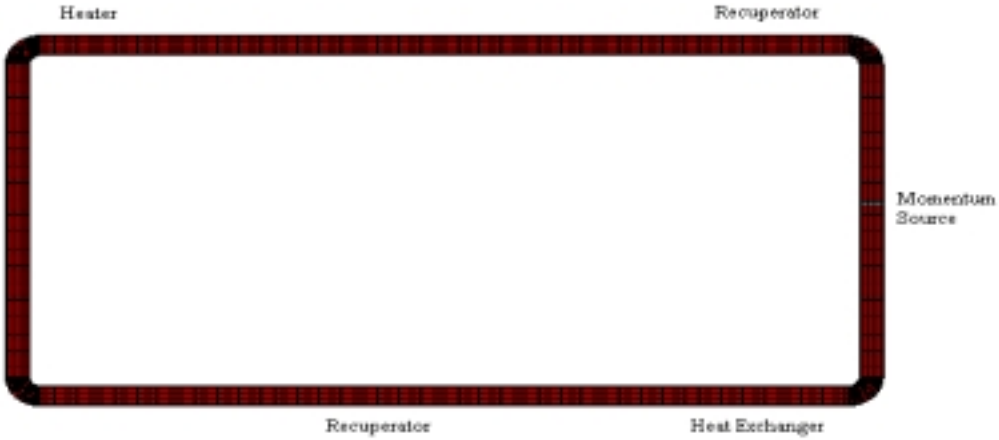

Figure – 14: Rectangular Loop Model

The model has been tested for both laminar and turbulent flow regimes the Reynolds' number being 2000 for the laminar flow and 200,000 for the turbulent flow. The velocity, temperature and concentration profiles at the elbow sections for each of these runs have been shown in the following figures. Figures 15 & 16 show the velocity profiles at the elbow section for the laminar ant turbulent regimes.

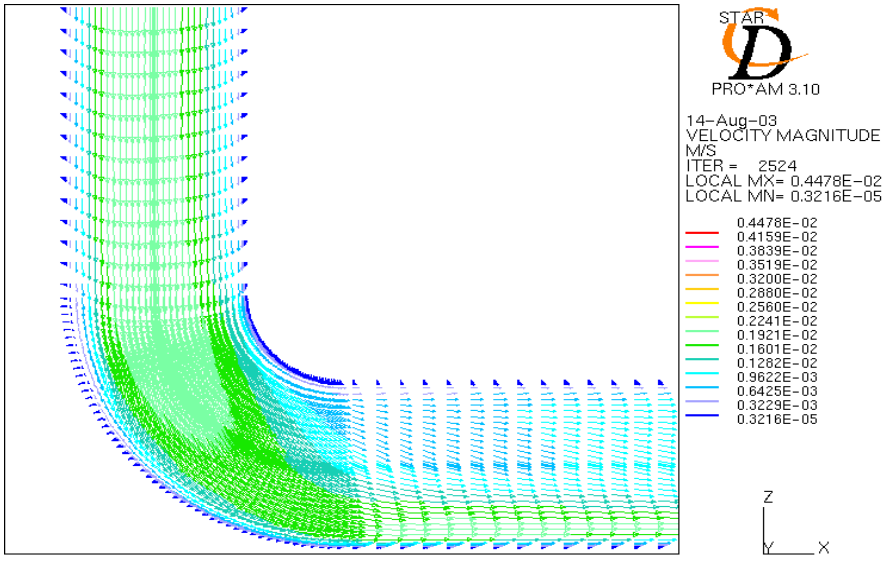

Figure 15: Velocity profile at an elbow section for the laminar flow in the rectangular loop model

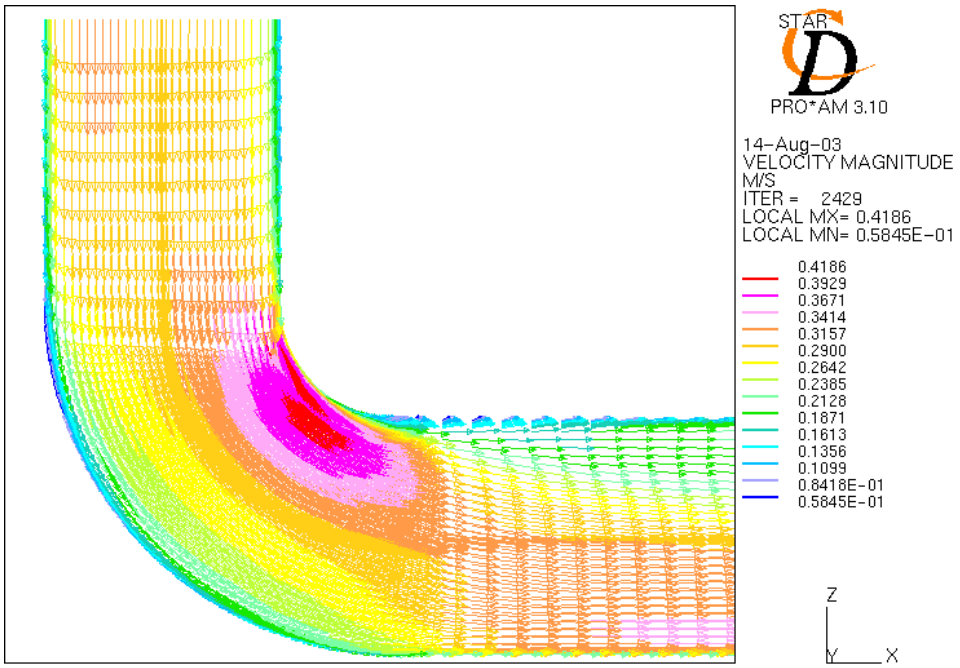

Figure 16: Velocity profile at an elbow section for the turbulent flow in the rectangular loop model

The temperature variation along the whole length of the loop for a laminar flow is shown in figure 17. The diffusion of temperature from the walls into the fluid is clearly seen all along the loop. Figure 18 shows the temperature distribution at an elbow section of the rectangular loop for a turbulent flow.

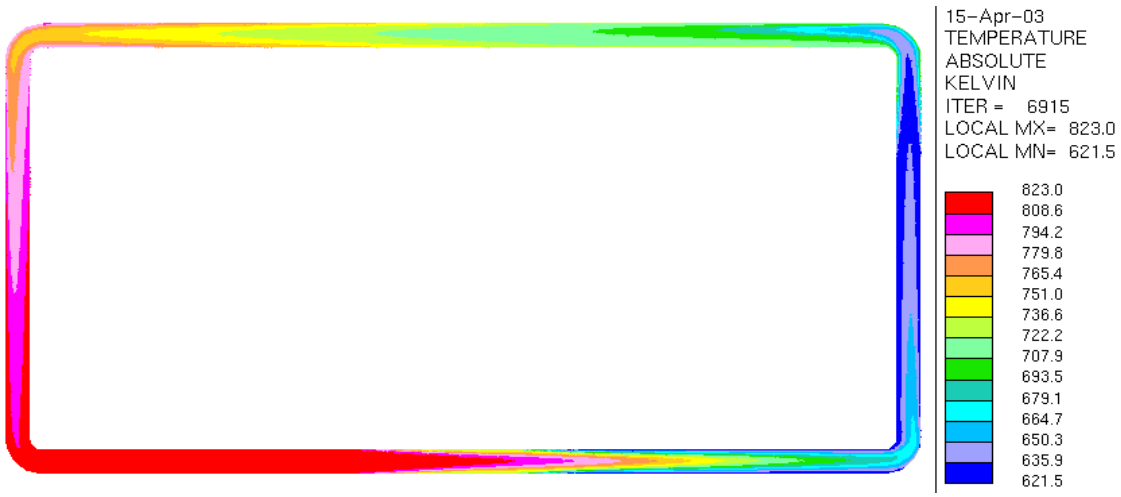

Figure 17: Temperature distribution for the laminar flow in the rectangular loop model

The diffusion in the lateral direction for laminar flow is more predominant than for the turbulent flow. This can be clearly visualized by comparing the left bottom corner elbow of figure 17 and the elbow in figure 18.

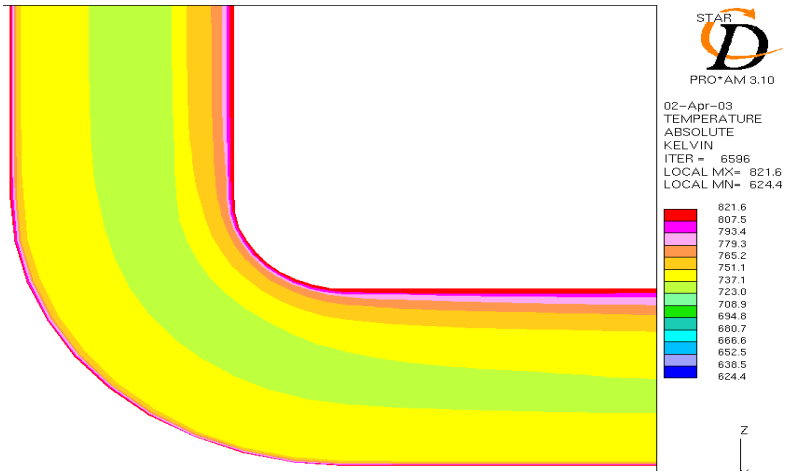

Figure 18: Temperature distribution for the turbulent flow in the rectangular loop model

Figures 19 & 20 show the concentration profiles for the laminar and turbulent regimes for the rectangular loop model. The above argument for the diffusion in the lateral direction holds good for this case as well and can be envisaged as did before by comparing the two figures.

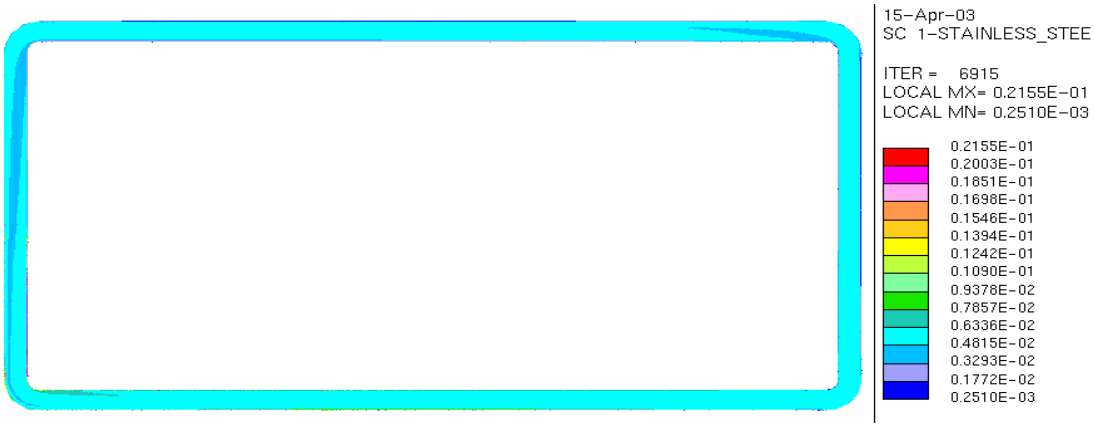

Figure 19: Concentration distribution for the laminar flow in the rectangular loop model

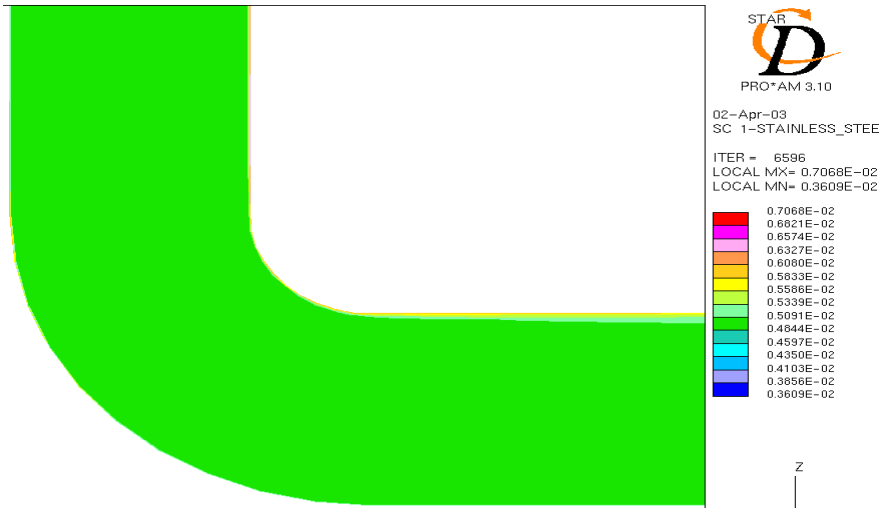

Figure 20: Concentration distribution for the laminar flow in the rectangular loop model

Benchmark and parametric studies have been carried out in both laminar and turbulent regimes. The results obtained from the benchmark study runs have been compared with the analytical results. Figure 21 shows the graph of concentration flux vs. loop length for the simulated model. For the current benchmark study for this model, the simulation results for the turbulent regime have been compared with the loop case with a temperature variation of 200°C in figure 7.

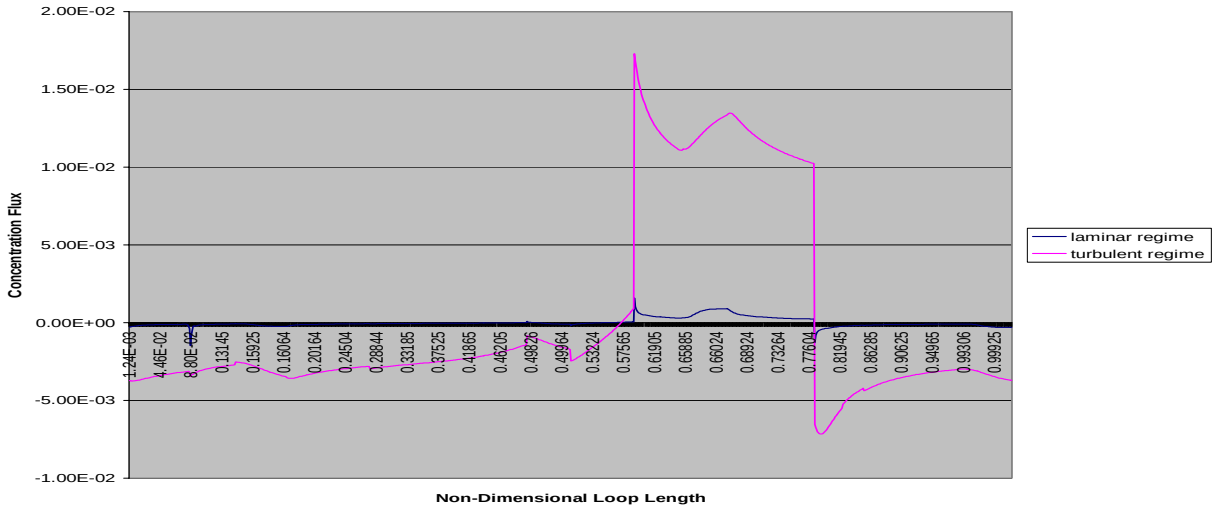

Figure – 21: Corrosion/precipitation rate for the closed rectangular loop model

It can be seen from figure 21, that the simulation results are very well in tune with the analytical results excepting at a few places where there are sudden falls and rises. These falls and raises can be observed at the non-dimensional loop lengths 0.15, 0.5, 0.65 and 1. This trend is due to the presence of the elbows at these locations. The concentration flux for the rectangular loop model is averaged at four points along the circumference of the pipe to take into consideration the effects of the bends at the elbows.

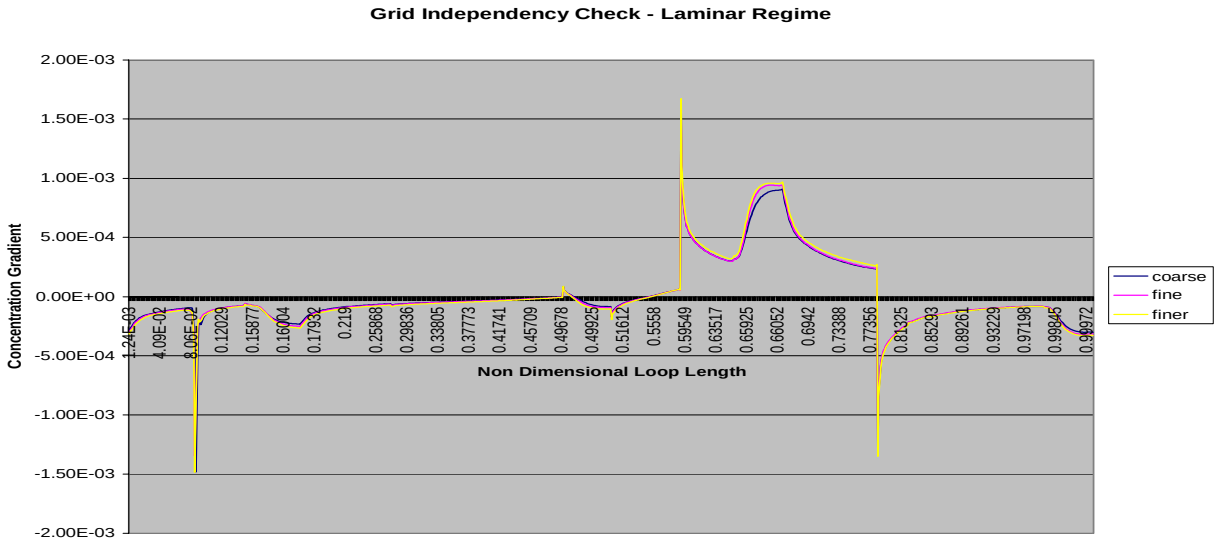

Figure – 22: Grid Independency Check for Laminar Regime

To check the grid independency for the benchmark study, three different mesh structures have been analyzed as has been done in the straight pipe model case. For all the three models, the concentration fluxes have been plotted again the loop lengths. The three plots are then compared with each other. The mesh distribution in the 'r', 'θ' and 'z' directions are as given below:

1. 24 X 10 X 1000
2. 24 X 20 X 1000
3. 24 X 30 X 1000

The results from the grid independence check have been plotted in figures 22 & 23. Figure 22 refers to the grid independency check for a laminar case flow and figure 23 refers to the turbulent flow grid independency check. The results from all the three mesh structures, for both the cases, have been put together in single graphs for easy comparison. The coarse, fine and finer meshes refer to the mesh structures 1, 2 and 3 above.

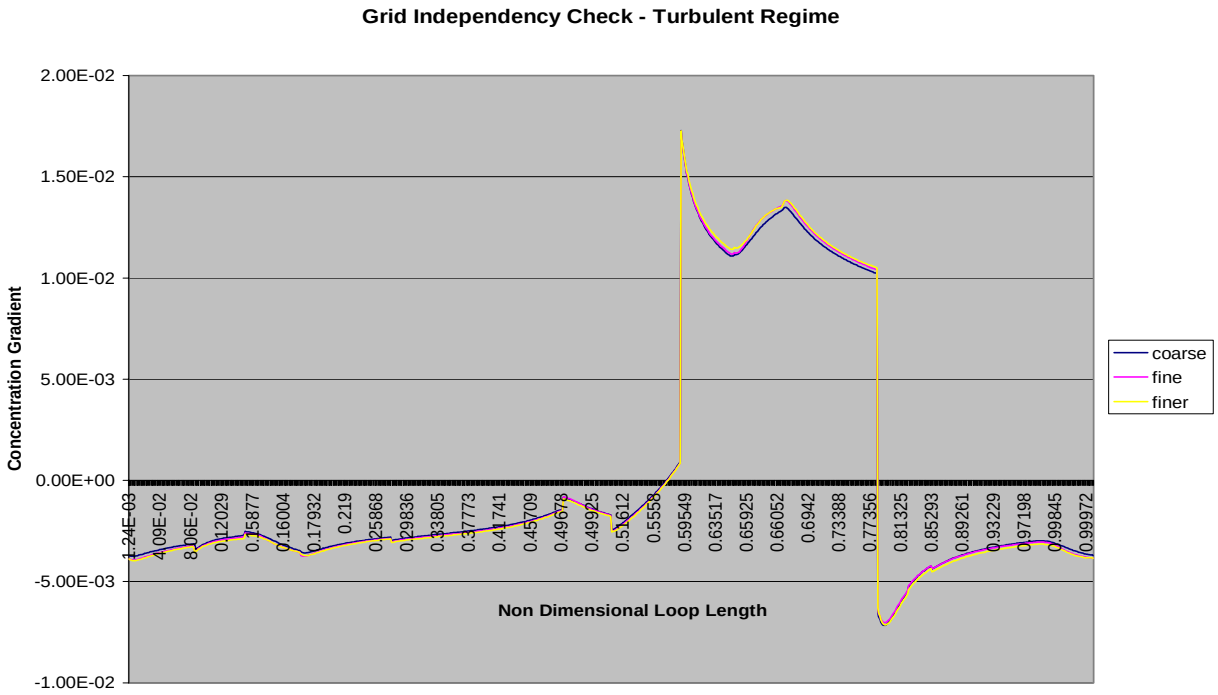

Figure – 23: Grid Independency Check for Turbulent Regime

As can be seen from both the figures, the concentration flux profiles for all the three mesh structures fall one on top of each other for both the laminar and turbulent regimes. Hence it could be deduced that the results are grid independent.

A parametric study has been carried out with the model with the minimum cells. The parameters that have been considered were Reynolds number, Schmidt number, initial oxygen concentration, and temperature variation along the loop length for the turbulent flow. The parameters considered for the laminar flow were Schmidt number, initial oxygen concentration and temperature variation along the loop length.

Parametric Study:

A parametric study has been carried out for the rectangular loop model with Reynolds number, Schmidt number, initial oxygen concentration and temperature variation along the loop length as parameters. The studies have been carried out both in the laminar and turbulent regimes. The parametric studies are mainly useful in determining the most critical points in the MTL i.e. the points of maximum or minimum corrosion and helps decide on the most favorable parameters to run the loop with longest possible life. The parametric study cases for each parameter have been analyzed separately in the following discussion.

Reynolds Number

Reynolds number plays a very vital role in the area of thermal hydraulics. It directly influences the mass diffusion rate in a pipe flow. The mass diffusion rate in turn affects the corrosion or precipitation rate in the MTL. Hence, the behavioral study of the mass diffusion with the variation of velocity makes a very interesting topic for the present case. For this reason, a parametric study of the Reynolds number has been carried out. The studies were limited to the turbulent flow because of the fact that the flow effects on mass diffusion are more predominant for high Reynolds numbers than for the low Reynolds numbers.

The parametric study consisted of flow modeling at five different Reynolds numbers. The range of Reynolds numbers considered were: 150000, 175000, 200000, 225000, and 250000. The simulations were carried out with all the remaining parameters kept at the pre-defined values for the benchmark study. Since the main focus of study is the corrosion / precipitation rate, the results of the concentration flux have been extracted. These results, from all the runs have been plotted against the non-dimensional loop length, as shown in the figure 24.

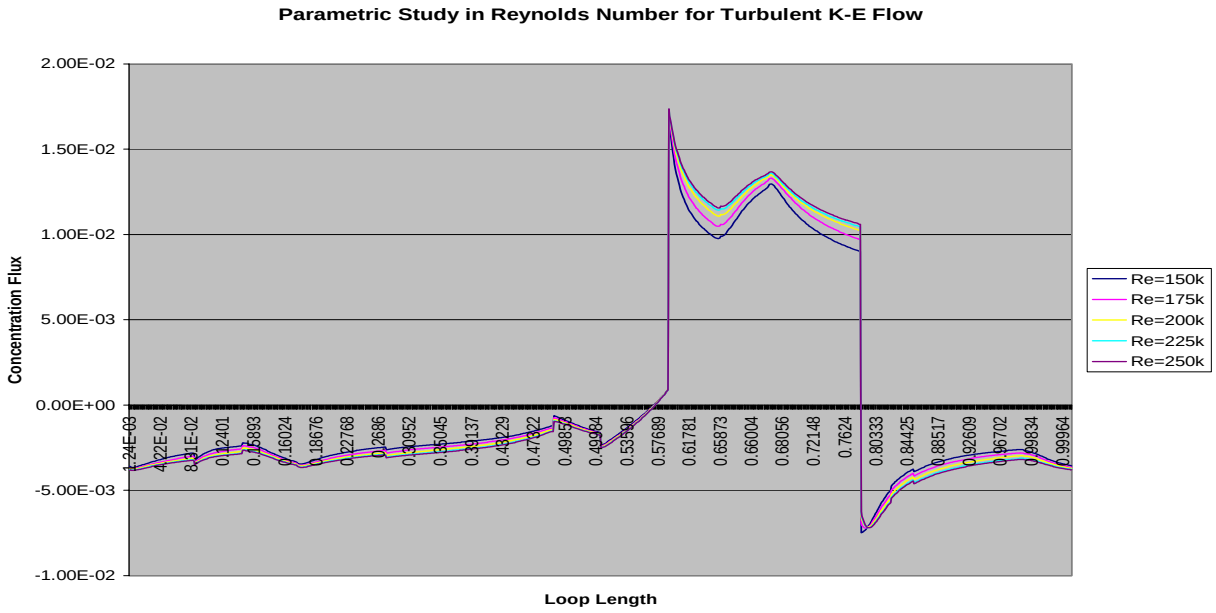

Figure – 24: Parametric Study in Reynolds Number for Turbulent K-ε Flow

As can be seen, the concentration flux from all the five runs almost overlap except at a few places. The maximal corrosion / precipitation point almost stays the same for all the runs. The only region where the variation is considerable is the region after the point of maximal corrosion and before the point of minimal corrosion. An elbow is present in this region and the region where the elbow is present has the maximum effect on the corrosion / precipitation rate. Apart from that, the effect of the Reynolds number in the given range is negligible on the corrosion / precipitation rate.

Schmidt Number

The next parameter considered for analysis is the Schmidt number. Schmidt number is the ratio of kinematic viscosity to diffusivity. For the parametric study, the kinematic viscosity has been kept constant and the diffusivity has been varied. The various Schmidt numbers considered were, 10, 50, 100, 150 and 200. The variation in the Schmidt number is expected to greatly influence the corrosion / precipitation rate since it is inversely proportional to the diffusivity. The study has been carried out for both the laminar and turbulent regimes. The other properties of the fluid for the analysis were kept constant and same as the benchmark study runs.

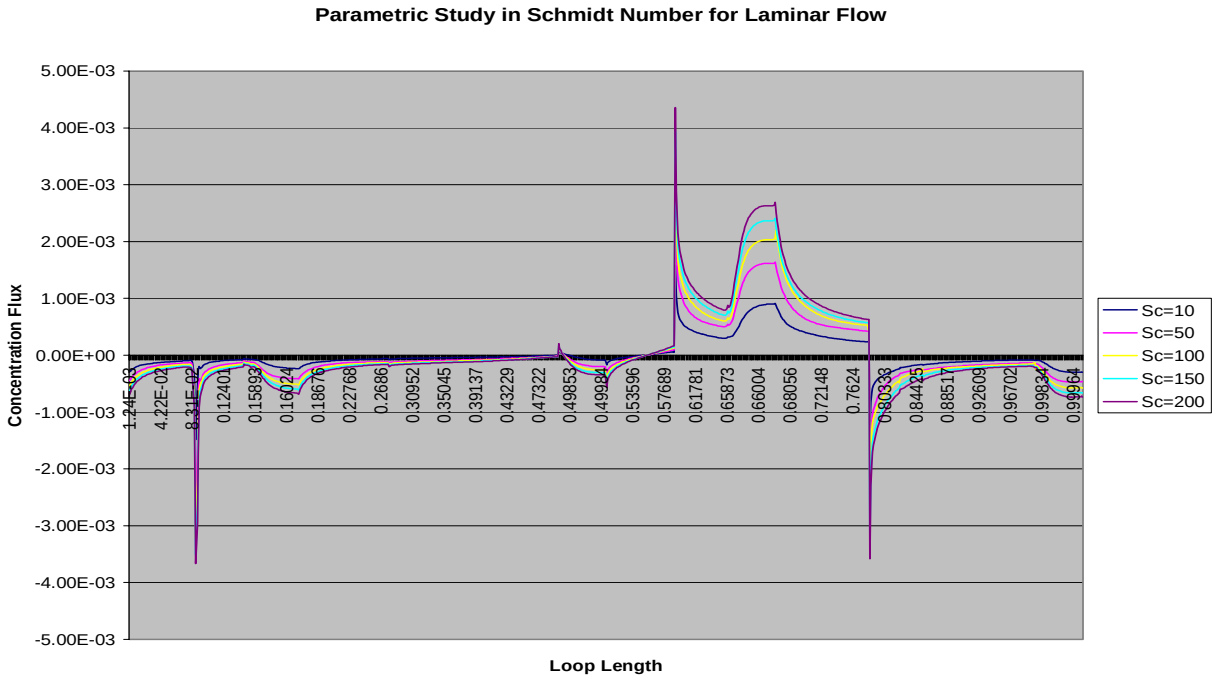

Figure – 25: Parametric study in Schmidt Number for Laminar Flow

Figure 25, shows the plot of variation of concentration flux with the non-dimensional loop length for laminar flow and figure 26 shows the same plot for the turbulent flow. It can be observed from both the figures that, higher the Schmidt number is, higher is the corrosion rate and lower is the precipitation. The points of maximum corrosion and precipitation, of course, are not affected by the variation. Hence, for longevity of the life of the MTL, the Schmidt number should be kept as low as possible.

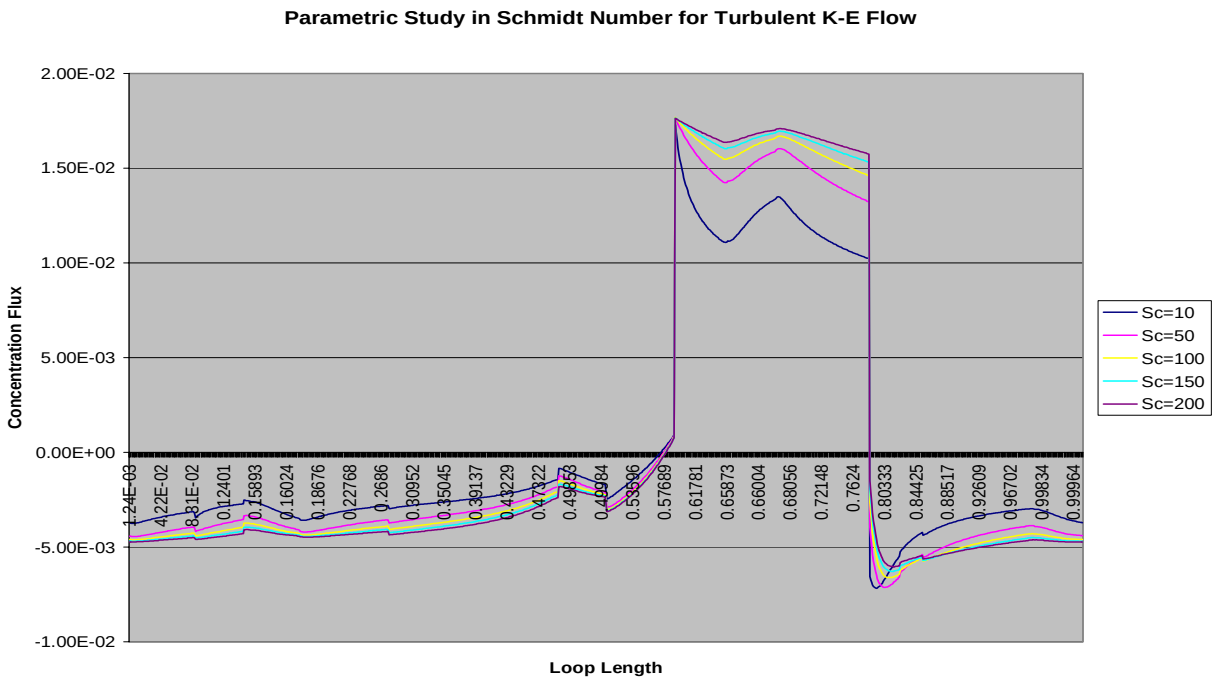

Figure – 26: Parametric Study in Schmidt Number for Turbulent Flow

Initial oxygen Concentration

The concentration of wall, as described before, is a function of initial oxygen concentration and temperature. The empirical formula is given by equation 7. The corrosion / precipitation rate is directly proportional to the wall concentration.

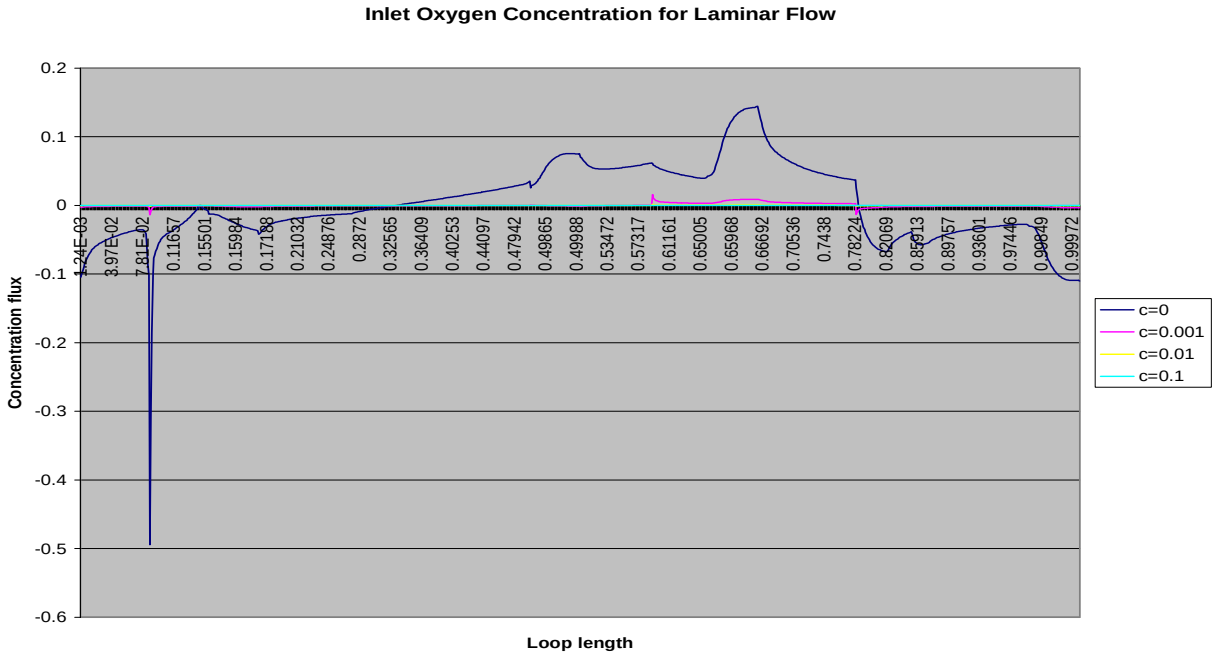

Figure – 27: Parametric Study in Initial Oxygen Concentration for Laminar Flow

Four different initial oxygen concentrations have been considered for the study. The simulations have been run both in the laminar and turbulent regimes. The initial oxygen concentrations that have been considered are 0.0, 0.0001, 0.001 and 0.1. Figures 27 & 28 show the variation of concentration flux with the variation of initial oxygen concentration for the laminar and turbulent regimes respectively. It can be clearly visualized that the initial oxygen concentration highly affects the overall corrosion / precipitation rate. Higher the oxygen concentration is, higher is the corrosion / precipitation rate.

The case where the initial oxygen concentration is zero has been analyzed for comparison purposes. It can be seen that by introducing an initial concentration greatly reduces the corrosion of the steel surfaces.

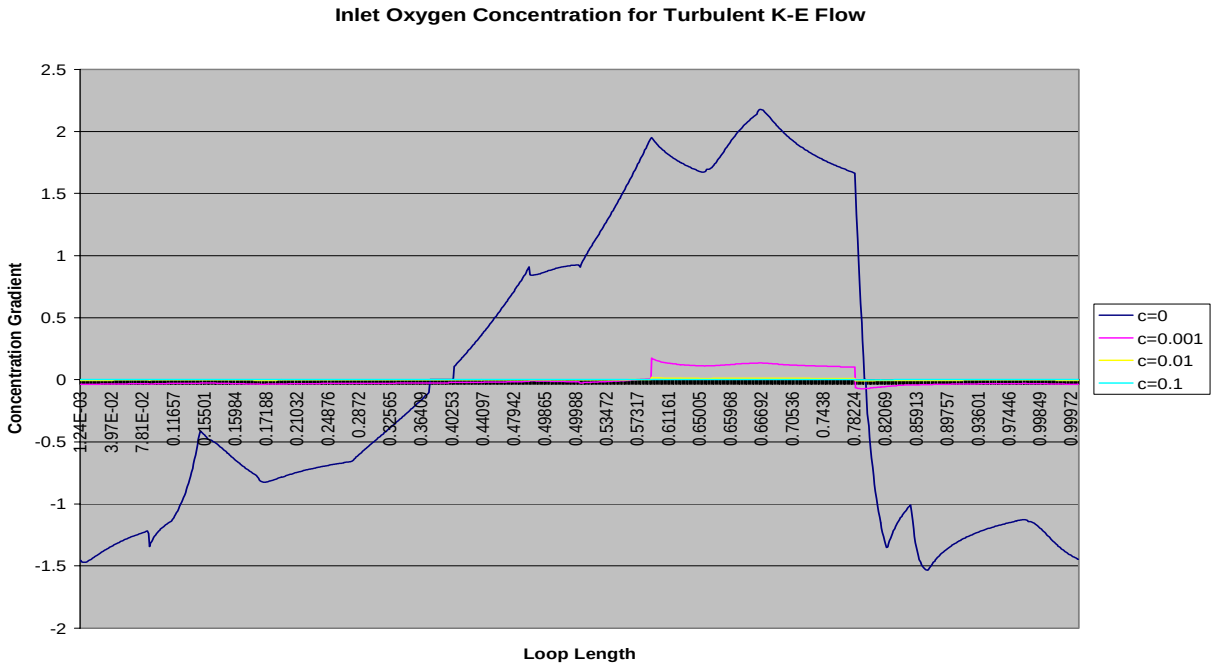

Figure – 28: Parametric Study in Initial Oxygen Concentration for Turbulent Flow

Temperature variation along the loop length

The final parameter considered for the parametric study is the wall temperature variation along the loop length. The wall concentration is a function of wall temperature, given by equation 7. Hence, by varying the wall temperature along the loop length has a direct of wall concentration, which in turn affects the corrosion or precipitation rate. For the benchmark study, the temperature gradient considered was 200^{o}C i.e. 350K – 550K. Five different temperature differences have been considered for doing the parametric study. The temperature gradients considered were, 50K, 100K, 150K, 200K and 250K. For all the five cases, the base temperature has been maintained at 350K. The imposed wall temperature trend along the loop length is also similar to the figure 2 for all the cases. The remaining parameters have been kept at the original conditions for the analysis. Simulations have been carried out in both laminar and turbulent regimes.

Figures 29 & 30 show the plot of corrosion / precipitation rate Vs the Loop length for various temperature ranges along the loop length for the laminar and turbulent regimes respectively.

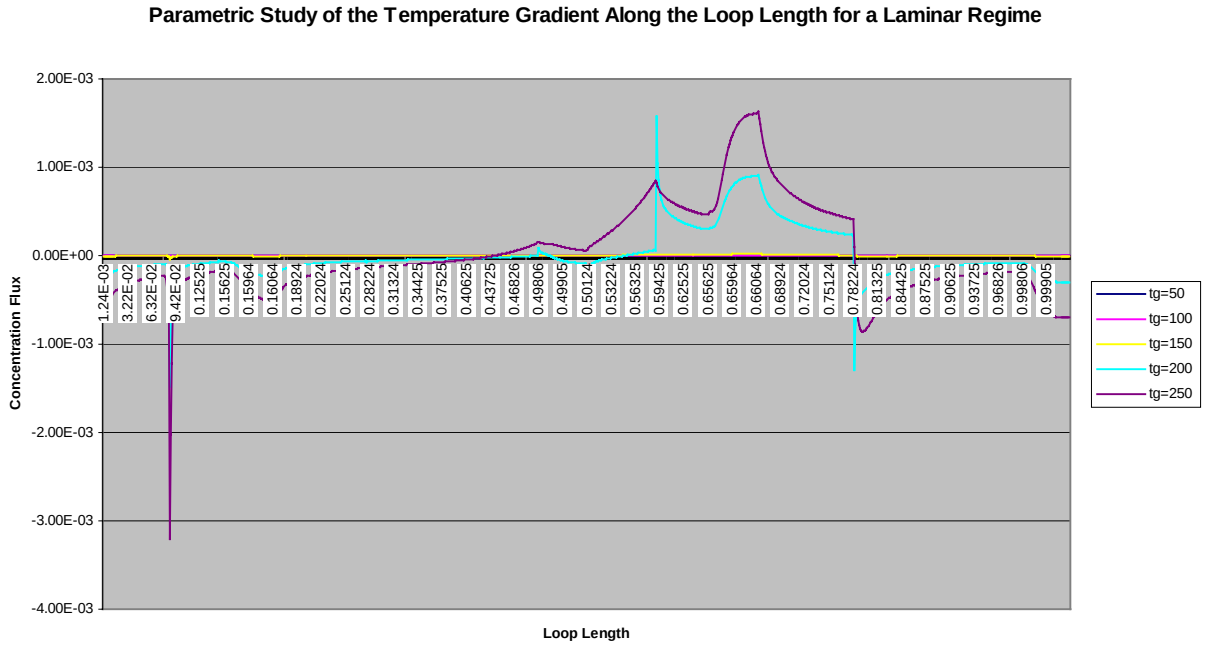

Figure – 29: Parametric study of the Temperature variation along the Loop Length for a Laminar Regime

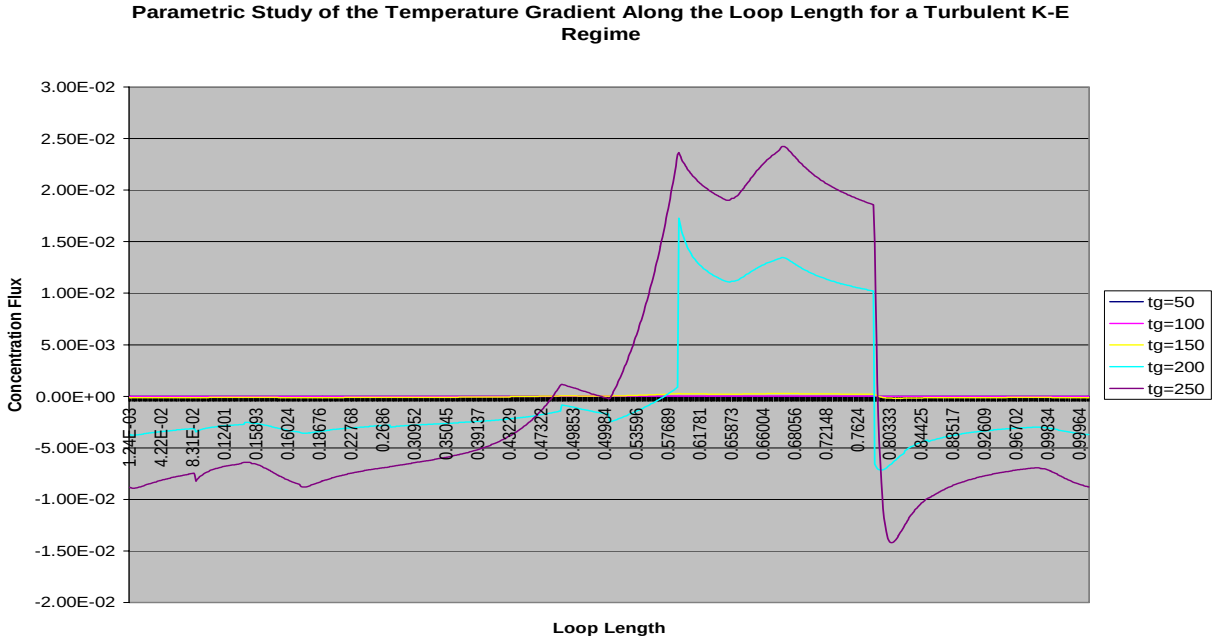

Figure – 30: Parametric study of the Temperature variation along the Loop Length for a Turbulent Regime

It can be deduced from the figures that the corrosion rate increases with the increase in the temperature gradient. The effect of temperature on the corrosion is very high. A 50K increase in the temperature highly increases the corrosion/precipitation rate as is obvious from the figure. Hence the temperature gradient should be kept at minimum possible levels for the long run of the loop.

Local Corrosion Modeling:

In this chapter, results obtained from self-developed code and commercial package, STAR-CD, are presented. Various parameters were chosen to study the effects on mass transport. The study covers both of laminar and turbulent regions and shows valuable significance to practical applications.

Results from Self-developed Code and Discussions

Benchmark

Benchmark is important in research, especially in numerical simulation. It provides the validation of the tools and the base for the further effort. Before used to carry out calculation for more complicated cases, the code was applied to a classic problem and compare outcome with widely accepted results. Incompressible flow in sudden expansions is one of the classical problems and suits our calculation domain perfectly.

Studies of separated flows in plane sudden expansions were documented previously by several authors. Acrivos and Schrader, Milo and Acrivos and Milos *et al.* have conducted extensive numerical studies of plane and axisymmetric sudden expansion flows and investigated the existence of steady solution to the Navier-Stokes equations for both parabolic and uniform inlet velocity profiles. Acrivos and Schrader carried out computations, on the basis of boundary layer equations, for several expansion ratios, and found that steady solutions exist for all values of the parameter λ, the ratio of the inlet channel half-width to the step height, when the inlet profile is parabolic. Milos and Acrivos carried out computations for a uniform inlet profile and several sudden expansion ratios. They used a global Newton method in order to circumvent the difficulties associated with the physical instability of the flow and their calculations revealed that the steady solution exists only if λ is below a critical value λ_c. Milos *et al.* presented detailed computations of the Navier-Stokes equations up to a Reynolds number of 1000 (based on the step height) for a uniform inflow past a cascade of sudden expansions. Their calculations revealed that for large values of the expansions ratio the eddy length increases linearly with Re, while for smaller values of the expansion ratio the solution of the Navier-Stokes equations, with increasing Re, approaches an asymptotic state for the eddy length.

Experimental and numerical results for axisymmetric, incompressible sudden expansion flows have been presented by Macagno and Hung at Reynolds numbers up to 200. Kwon *et al.* and Kumar and Yajnik studied numerically sudden expansion flows using the boundary-layer equations while Navier-Stokes calculations for symmetric flows past a sudden expansion have also been reported by Hung and Morihara and more recently by Scott *et al.* Napolitano and Cinnela *et al.* and Hawken *et al.* Recently, Baloch *et al.* have also conducted a numerical study

of two- and three-dimensional expansion flows based on the Navier-Stokes equations and a semi-implicit Taylor-Galerkin/pressure-correction finite element scheme, but the computations were limited to very low Reynolds numbers and no attempt was made to calculate flow bifurcations.

Early experimental studies by Durst *et al.* of low Reynolds number flows over 1:2 and 1:3 plane expansions revealed asymmetric separation beyond a certain Reynolds number. The ratios mentioned in this thesis are the height of inlet to the height of expanded area. A further experimental study of flow in the same geometries was performed by Chedron *et al.*, demonstrating that symmetric flow in symmetric sudden expansions can exist only within a limited range of Reynolds numbers. Chedron *et al.* performed flow visualization in order to obtain time-averaged information about the various flow regimes near the sudden expansion. Under the conditions of an expansion ratio of 1:2 and grid aspect ratio of 8, they observed that the flow became asymmetric at Reynolds numbers higher than 185 based on the maximum velocity and upstream channel height. Another experimental and numerical study of the flow in symmetric sudden expansion, with expansion ratio 1:3, was published by Fearn *et al.* Their results were verified by Shapira *et al.*, who performed a linear stability analysis of symmetric flow in plane sudden expansions. Shapira *et al.* found a critical Reynolds number Re_c of 82.6 (based on the maximum velocity and upstream channel height), which is in good agreement with the results of Fearn *et al.* for an expansion ratio of 1:3 (Fearn *et al.* reported Re_c=40.45 based on the upstream channel half-height, i.e. Re_c=80.9 based on the upstream channel height.) Drikakis numerically studied this sudden expansion problem and performed computations at various Reynolds number and expansion ratio, which turns out to be a good reference to compare with.

Figure 31 shows different flow behaviors according to different Reynolds numbers at expansion ratio of 1:6. When Reynolds number is low, flow develops symmetrically. While the increase of Reynolds number to certain point, symmetry is broken and bifurcation is observed. In this case, this critical Reynolds number turns out to be 25. Finally, Reynolds number is getting too big for flow to keep steady. More vortexes are generated from corner and spread to downstream along the wall.

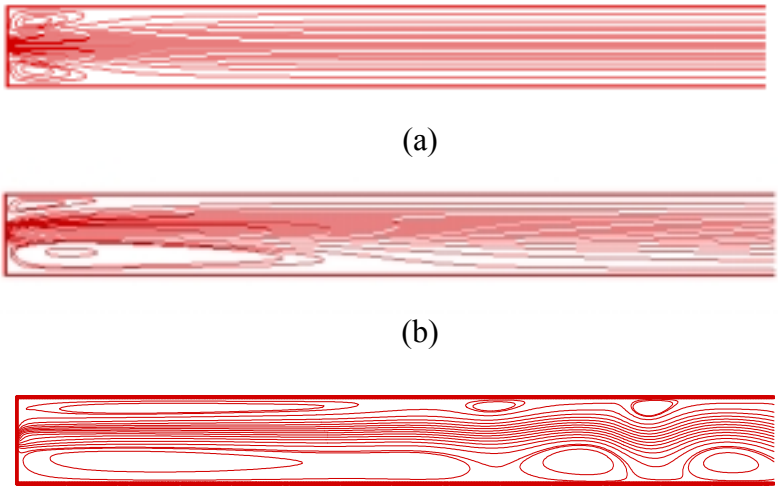

(a)

(b)

(c)

Figure – 31: Streamlines for Reynolds numbers equal to (a) 10, (b) 30 and (c) 150

It should be noted that the third picture in Figure 31 is distorted to give a better visual effect in limited space. The size of vortexes and the position of them are different from what and where they appear to be.

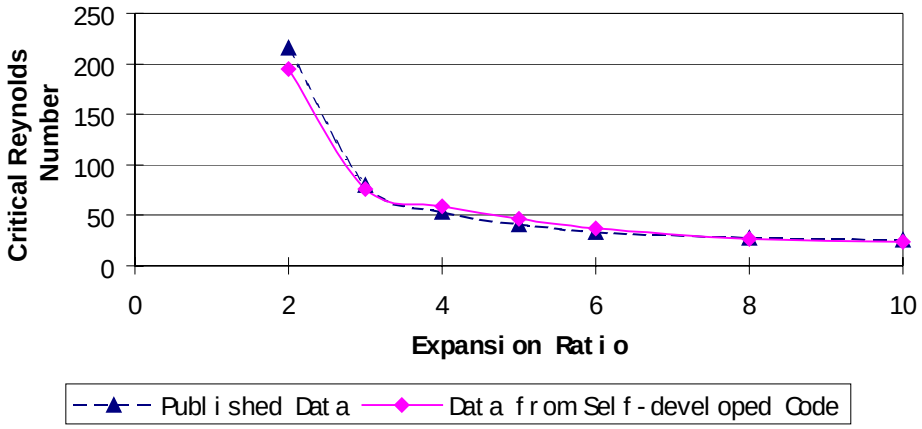

Figure – 32: Comparison of expansion ratios vs. critical Reynolds numbers between current study and Drikakis

Similarly, more expansion ratios were considered. Different critical Reynolds numbers were obtained to benchmark with published results. Figure 32 depicts how the curves of critical Reynolds number obtained from both self-developed code and published results look like along expansion ratio. Drikakis used maximum velocity of fully developed flow in the definition of Reynolds number, while average velocity was chosen in self-developed code. In light of this discrepancy, conversion has been done to Reynolds number so that the values from two sources are comparable. As can be seen from figure, two curves are very close to each other and the maximum of relative error is around 10%. Considering different numerical methods and order of accuracies involved, the results from self-developed code are reasonable and credible.

Results from Self-developed Code and Discussions

In practical problem, corrosion takes place on the inner surface of loop. He *et al.* published an empirical formula to prove that contaminants generated are function of local temperature and the concentration of reactants. In the code, temperature was not taken account of. Uniform concentration of species was assumed as boundary condition at wall. In this way, continuous generated species whose movement is greatly affected by flow are modeled. As the products of corrosion, species move under both effects of diffusion and convection. The code reveals these complicated phenomena by solving governing equations aforementioned.

A numbers of factors affect mass transfer and corrosion rate by varying concentration gradient, especially when corrosion happens in the environment which involved complicated flow movement. Because of the truth that complicate flow situations always take place in the region close to corner and wall in this kind of sudden expansion geometry, the concentration gradient on the wall surface is of more importance than that in bulk region. Vortices and circulation disturb the formation of boundary layer. Consequently, theoretical estimation of mass transfer phenomenon is not applicable and more uncertainties need to be considered in those

kinds of situations. Flow pattern decides the way how species is washed from the wall and diffuses into bulk region. In the code, concentration gradient at wall is calculated according to expression $\frac{C_{wall} - C_{wall-1}}{\Delta y}$. In the light of unsteady nature of flow, at each cross section, concentration gradients on upper and bottom wall are taken average to show general idea of how species is transported at near-wall region along the distance to inlet.

Work was basically carried out with the parametric study of several factors, such as Reynolds Number, expansion ratio and Schmidt Number. Different combinations show how those factors affect species transfer.

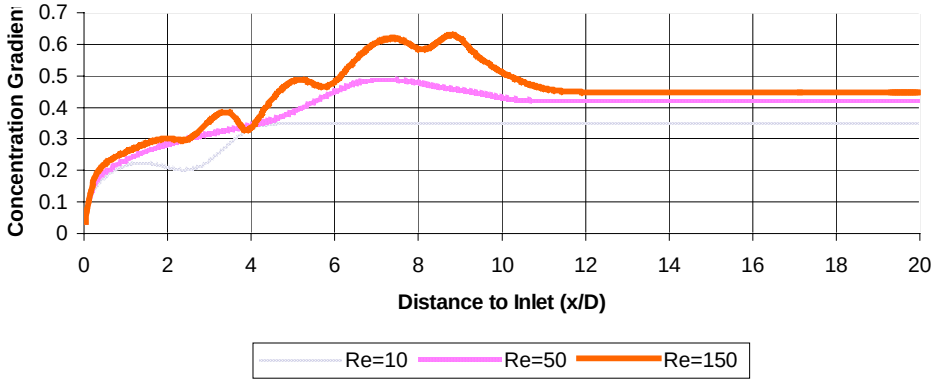

Figure – 33: Concentration gradient vs. distance to inlet at expansion ratio of 10

Expansion Ratio

To find out the effects on mass transfer brought in by expansion ratio, three ratios were chosen to look at. They are 3, 6 and 10. Figure 33, 34 and 35 show the concentration gradients at different Reynolds Number at each expansion ratio versus distance to inlet. The results are obtained after certain amount time elapses. They are results at one instance, not averaged over time.

From those figures, we can tell that, at each expansion ratio, higher Reynolds Number generally yields higher concentration gradient. When Reynolds Number is very low, like around 10, concentration gradient varies smoothly from inlet to a certain distance and reaches its maximum value. After that point, it remains at the same value. While Reynolds Number goes up, flow becomes unsteady. Instead of smooth curve, lines start oscillating and contain numbers of peaks along x coordinate. It is because of vortexes and circulations disturb the formation of boundary layer. In near wall region, each re-circulation zone affects mass transfer to a similar pattern, which is the reason why figures show several peaks with the shape close to each other. The difference between each of those oscillations in value and width is brought in by upstream which varies from one to another. One thing need to be noticed is, even though, concentration gradient lines of higher Reynolds Number in those figures seem to reach a steady situation, it is believed due to the inadequate computational time. Given more time steps, vortexes and

circulations will spread to downstream along the wall. Time step is calculated according to $0.01 * \Delta x * \Delta y$, as suggested.

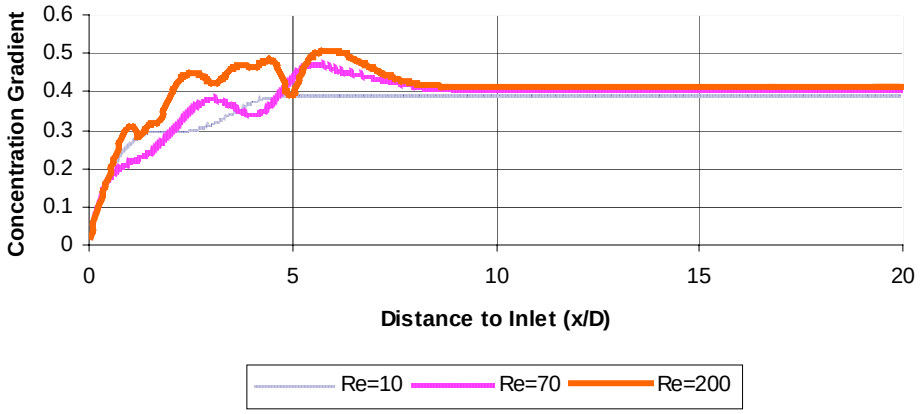

Figure – 34: Concentration gradient vs. distance to inlet at expansion ratio of 6

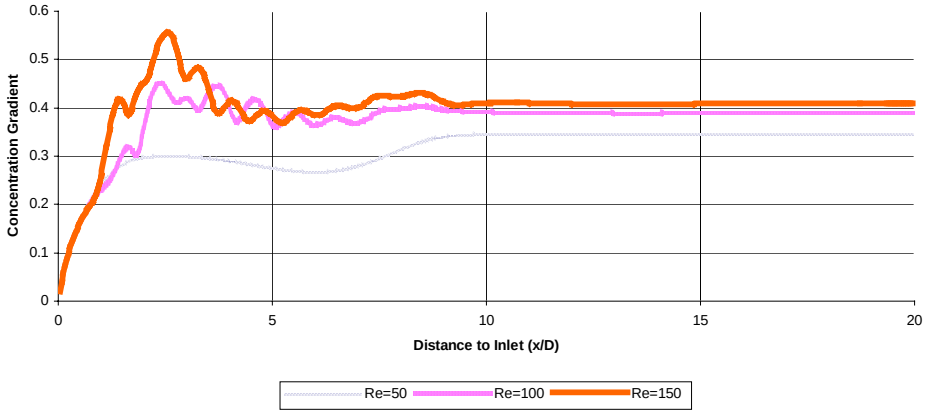

Figure – 35: Concentration gradient vs. distance to inlet at expansion ratio of 3

It is also can be observed that for the same expansion ratio, maximum of concentration gradient for those relatively high Reynolds Numbers occurs almost at same distance to inlet, while the value of maximum differs in the same order. With the increasing of expansion ratio, the distance to inlet where biggest concentration gradient occurs is pushed downstream. Figure 36 depicts the trend between peak location and expansion ratio.

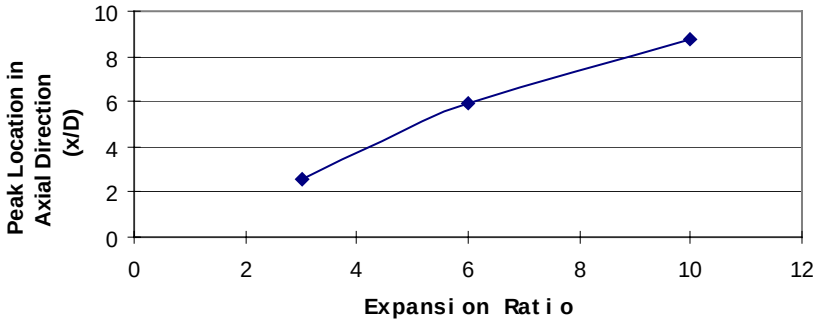

Figure – 36: Peak locations in axial direction for different expansion ratios

It can be concluded that, at same expansion ratio, higher Reynolds Number will bring higher concentration gradient so that corrosion will be more likely to happen. As far as expansion ratio, it will not change the scale of concentration gradient too much, but the place where maximum gradient occurs. Figure 36 reveals that the location of greatest gradient increases when expansion ratio becomes bigger.

Schmidt Number

From the definition given before, Schmidt number is equal to $\frac{\upsilon}{D}$, which is the ratio of viscosity and diffusivity. The value of Schmidt number affects mass transport significantly. So, parametric study on Schmidt number was also carried out.

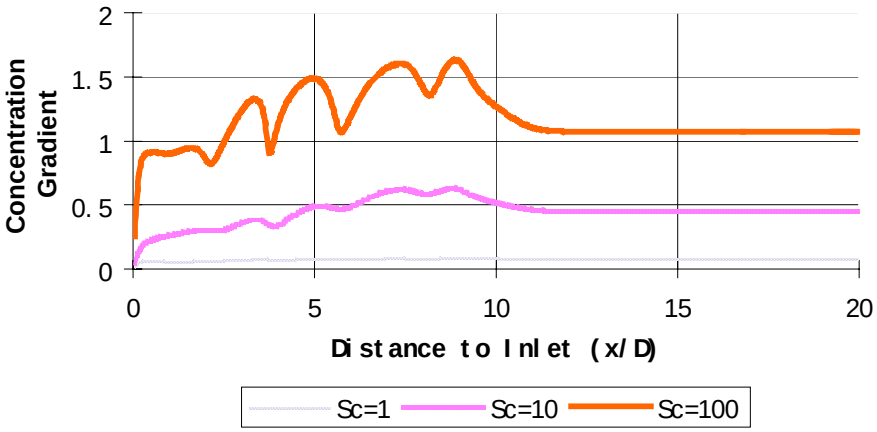

Figure – 37: Concentration gradient vs. distance to inlet at different Schmidt number

In Figure 37, three curves represent concentration gradient variation along the distance to inlet at same Reynolds number of 150 and expansion ratio of 10 but different Schmidt numbers. As we can easily observe, higher Schmidt number yields higher concentration gradient. It is harder for species to diffuse inside to the bulk region than to be washed away by flow. As a result, the lower the Schmidt Number is, the less corrosion will happen, according to the scale of concentration gradient.

Results from STAR-CD and Discussions

Model Setup

Study was carried out in 2-D models at this early stage. As shown in Figure 38, studied problem was given sudden expanded geometry. Temperature along the length of the plate is assumed constant. A uniformly generated mesh is used, which means the length and height are divided into equally spaced grids. Different mesh sizes were tested to check the mesh independence. Results on these tests are included later. Initially, flow does not contain any species at inlet, while two plates have a fixed concentration of species. In this way the species on the plates will diffuse into the bulk region, and the expected corrosion rate along the length may vary due to the difference of local flow condition and concentration profiles normal to the wall. Engineering unit here for the model is not important. Dimensionless scale is used in Figure 2.8.

Inlet height, d, is 0.5, the height of expanded area is 1.0 and the length is 10. C_{wall} is set at 0.5 for both plates. LBE is allowed to flow from inlet. All the physical properties of flow are listed in Table 2.

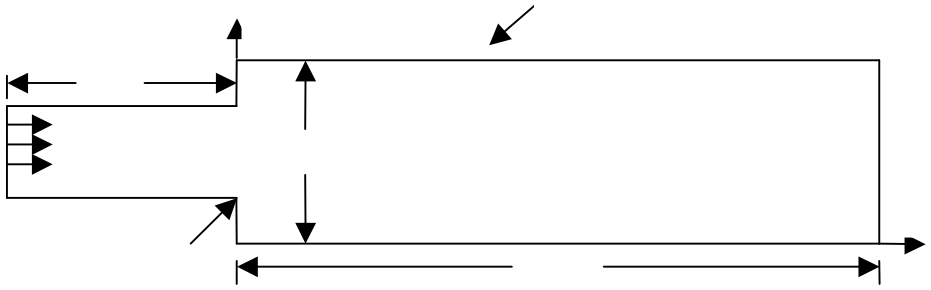

Figure – 38: Schematic of sudden expansion geometry

Table 2 Physical Properties Used in Study

	Magnitude
Density	10120.3 kg/m^3
Molecular Viscosity	0.003941 kg/ms
Diffusivity	10^{-9} m^2/s
Schmidt Number	389

Meanwhile, it has been well accepted that Hopf bifurcation occurs in this kind of symmetric sudden expansion domain, when Reynolds number reaches certain critical value. Oscillation or vibration appears in the flow and the resultant flow becomes unsteady and periodic in time. To verify that, one monitoring cell was assigned at location (d, d), according to Figure 38. Figure 39 proves that U-Component of velocity at monitoring cell oscillates and shows a periodic pattern. In addition, Figure 40 gives a direct idea how flow propagates along time. All those data and results are from the flow whose Reynolds number is equal to 1000.

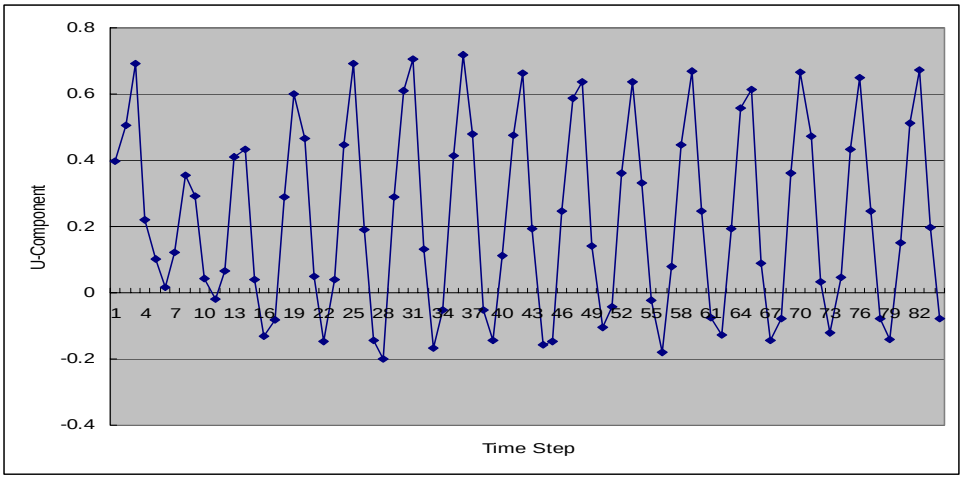

Figure – 39: U-component of velocity of monitored cell at Re equal to 1,000

Mesh Independence

Mesh independence is a crucial step for numerical simulation. It guarantees code and algorithm to produce as accurate results as it can and, at the same time, removes errors brought in by using different mesh sizes. A grid sensitivity study was performed using three grids: 400*100, 600*150 and 800*200.

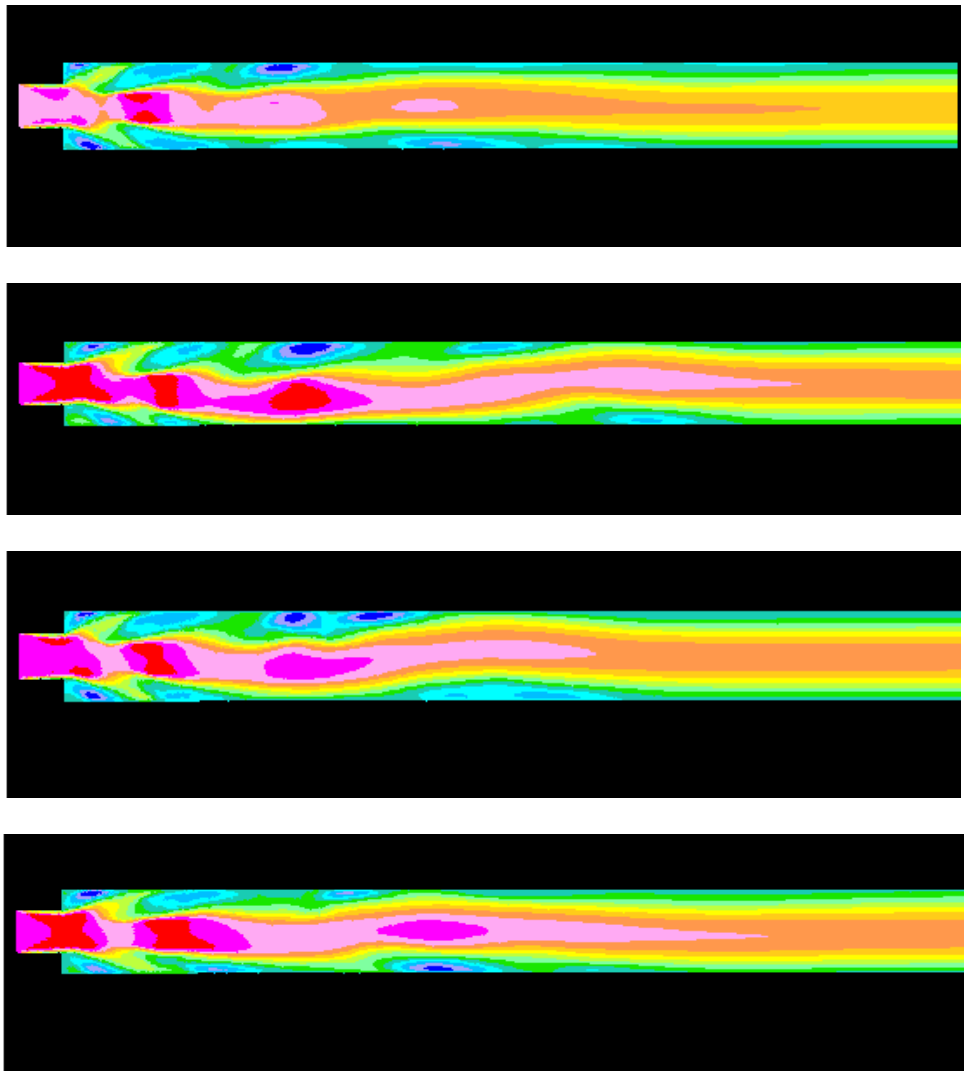

Figure – 40: Fluctuation of U-component of velocity

The geometry of testing model is same as before, a 2-D sudden expansion with ratio of 1:2. Reynolds Number is chosen as 1000. And, two points with coordinates (0.75, 0.5) and (1.0, 0.5) are picked as monitoring spots in each mesh size. To save calculation time, only part of domain, which is four times of expanded diameter long in axial direction starting from expansion, is revised by giving different mesh sizes.

Results from three mesh sizes are presented in Figure 41 and Figure 42. Again, U-component of velocity was monitored to plot the variation over time step. From two figures, the

blue line, which stands for coarsest mesh, 400*100, is obviously far from the other two. While pink and yellow lines are quite close to each other. Both of them captured similar fluctuation. The phase of wave almost keeps oscillating in an identical way. The values at each time step are fairly close as well. After the analysis of results in aforementioned three mesh sizes, the one with medium mesh density, e.g. 600*150, was selected to be used for further study. In this way, credibility of results can be ensured very well without paying too much computational time for higher fineness of mesh.

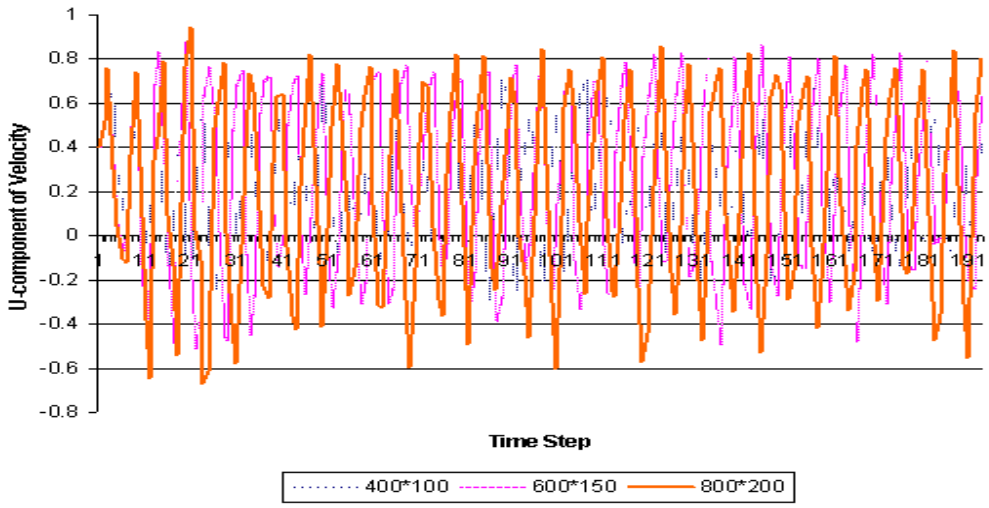

Figure – 41: U-component of velocity of point one in different sizes of mesh

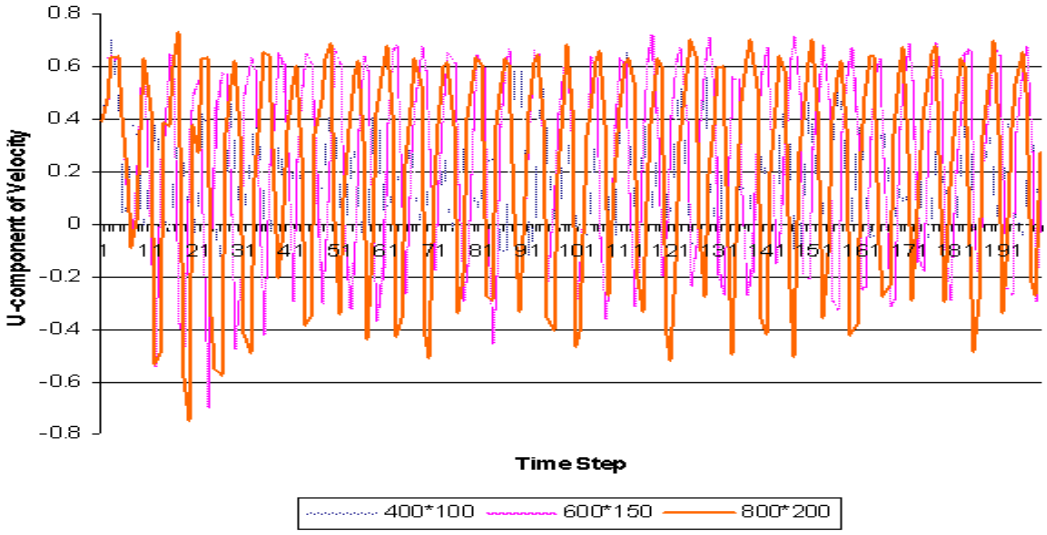

Fig – 42: U-component of velocity of point two in different sizes of mesh

To answer the question why there is a noticeable difference between pink and yellow curves, the reason is the Reynolds number. With the increase of Reynolds number, flow becomes more unsteady and fluctuates more dramatically. In the results showed above, Reynolds number 1000 was employed. It is a relatively high, even though it is still in laminar region. For this kind

of flow, it is much harder to bring the discrepancy among different mesh sizes down to negligible level. Considering these aspects, the medium mesh size is taken acceptable.

Results and Discussions

Mass Transfer Coefficient

Mass transfer coefficient, k, is the parameter used to measure mass transport phenomenon. In this case, it can be defined as:

$$k = \frac{D_{coeff} \cdot \Delta C}{\Delta y \cdot C_{wall}} \qquad (8)$$

where ΔC is the concentration difference between wall and the first cell next to the wall, and Δy is half height of that cell, since value of parameters in finite volume method is calculated at center of each cell, instead of each node in other methods.

From Equation 8, mass transfer coefficient can be obtained at given x location. Data collected from different locations is plotted to reveal how mass transport is changed in axial direction by geometrical difference.

Due to the periodic nature of the flow at high Reynolds numbers, mass transfer coefficient at every location is time-averaged, which means data of each point are collected at several times on both of upper and bottom wall within one period and then taken average. This guarantees results more accurate in a long time scope and smoothes out some misleading information brought in by instability.

After geometry was set up, physical properties were assigned and boundary conditions were given, a model is ready to study on the mass transfer coefficient variation along the distance to expansion inlet. STAR-CD does not have built-in function to calculate mass transfer coefficient automatically. The raw data was extracted from STAR-CD and analyzed and plotted manually. STAR-CD has a limit for the number of values you can edit at same time, which is 1,000. Since each layer of nodes in x direction exceeds this number, data from first ten times of expanded diameter (10D) starting from expansion inlet were collected for the convenience.

Two Reynolds numbers, 1,000 and 24,000, were chosen to use. Consequently, both of laminar and turbulent flow is covered in the study. It can be observed that mass transfer coefficient varies with the distance after sudden expansion.

Two ways of averaging data over time were considered. The first way used is to separate the layer of cells which are next to walls, both of upper wall and bottom wall, at certain one time step and then get the concentration value of each of those cells. By doing this, we can subtract the value at each cell from the concentration at wall, which is uniform in this case, and get the ΔC . Easily, mass transfer coefficient in axial direction is obtained at upper and bottom walls, according to Equation 8. Average the pair of values having same x coordinates and get the mass transfer coefficients at one time step. Repeating doing this at different time steps gives multiple sets of data. Finally, take the average out of those sets of data. The final values are considered time-averaged. Figure 43 and 44 show the output using this method. The drawback of this

method is time-consuming work and low efficiency, which prevent a more accurate estimation. Results in Figure 43 and 44 are the averaged ten different time steps.

Figure 43 is mass transfer coefficient plotted at Reynolds number of 1,000. It reaches peak from starting value very quickly at around 1D and then decreases to smaller numbers at a nearly fixed slope. The peak value at 1D is almost four times of minimum. And the coefficient remains at a high level in the region close to expansion.

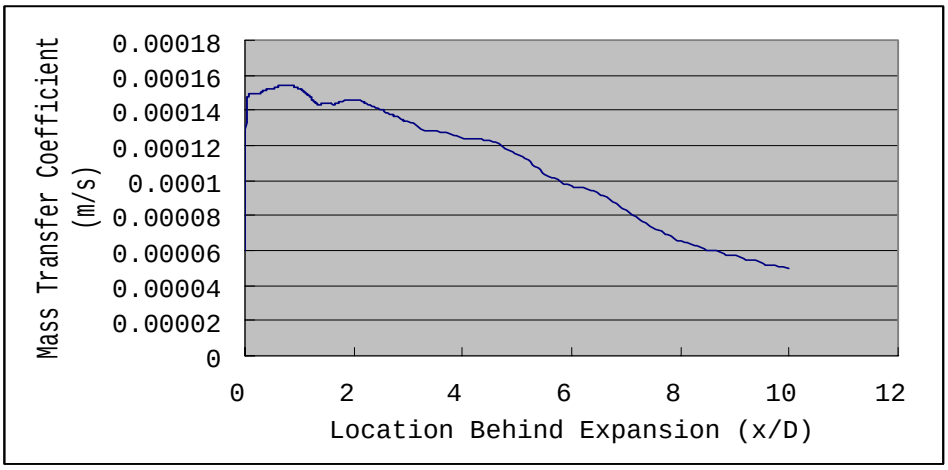

Figure – 43: Mass transfer coefficient variation at Re=1,000

Figure 44 is obtained when Reynolds number at 24,000. High velocity flow enhances the species transfer. Comparing to Reynolds number of 1,000, coefficient values are approximately twice higher. However, the complicated nature of turbulent flow makes mass transfer more instable and unpredictable. Vortexes and reattchments can greatly intensify local species transfer, due to higher velocity in those circulation zones. At such a high Reynolds number, locations of vortexes and reattchments are constantly moving with the propagation of flow which gives rise to the irregularity. Similar to laminar case, the region close to expansion, from 0 to 2D, has largest values in the whole domain. Mass transfer rate tends to decline, though there are a couple of sub-peaks in downstream.

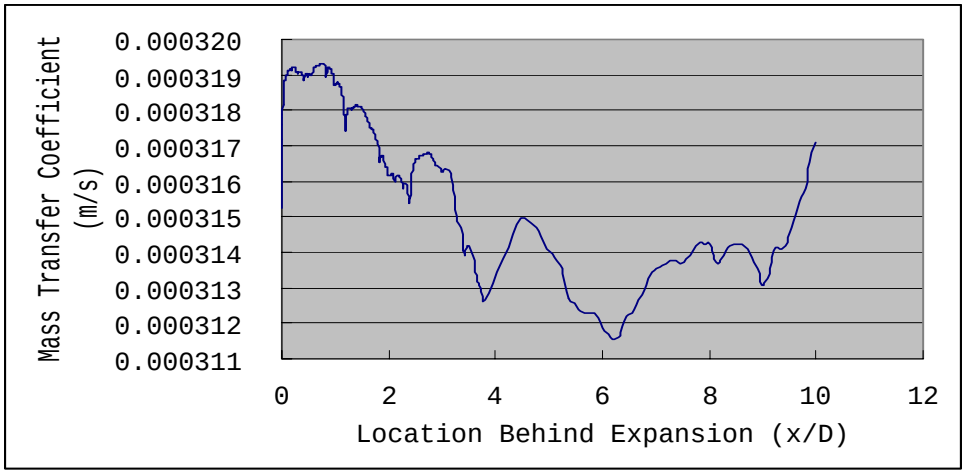

Figure – 44: Mass transfer coefficient variation at Re=24,000

The second idea on how to average data is gotten from experiment, which uses electronic sensors to collect data over a time range. Similarly, twenty cells at locations of interest were saved in a .set file in STAR-CD. With cell monitoring feature in STAR-CD, concentration values of each time step at those cells can be saved in another .ecd file. It is easy to edit those values and get the average over whatever the time range needed. The restriction of this method is only limited cells can be monitored, which means the plots made out of those values are simple and rough. Figure 45 and Figure 46 show the results of mass transfer coefficient.

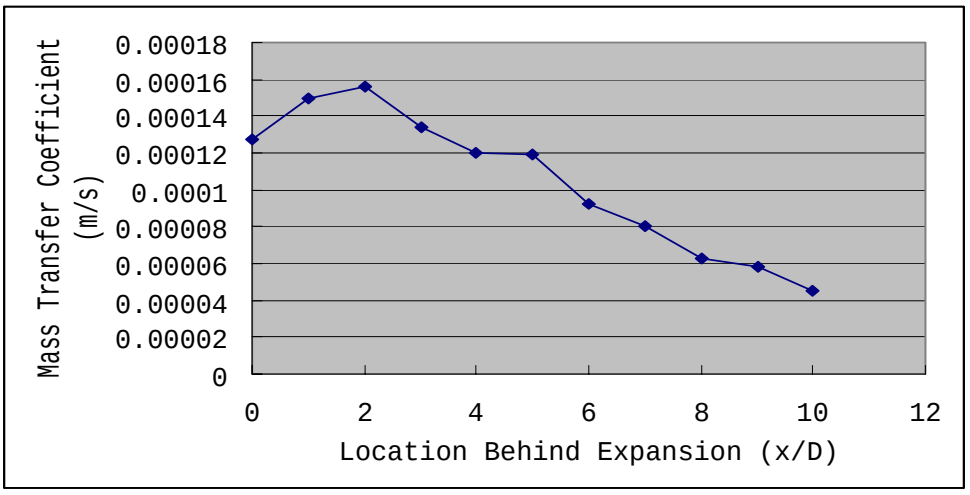

Figure – 45: Mass transfer coefficient variation at Re=1,000

The curve for Reynolds Number of 1,000 appears to be close to the plot obtained using first method, e.g. Figure 43. While for Reynolds number of 24,000, Figure 46 shows quite a different picture from Figure 44. Actually, according to the work from Rizk *et al.*, Figure 46 provides a better estimation than Figure 44, because for higher Reynolds number and more unsteady flow, 10 samples of data is not adequate for even a close approximation.

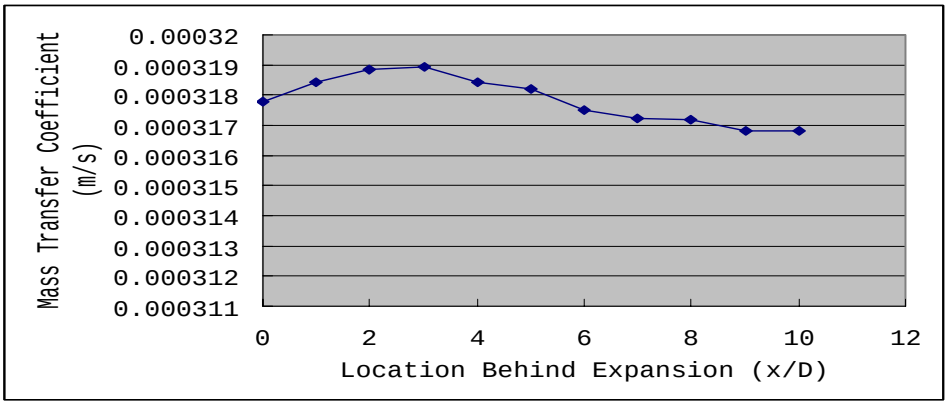

Figure – 46: Mass transfer coefficient variation at Re=24,000

REFERENCES

1. R.G. Ballinger, J.Y. Lim, 2001, Research Activities in US Related to Material Compatibility Issues for Nuclear Systems Using Heavy-Liquid-Metal Coolant.
2. W. Blatt, T. Kohley, U. Lotz and E. Heitz, 1989, *Corrosion* 45, 793.
3. J. Buongiorno, N.E. Todreas, M.S. Kazimi, "An Oxygen Control Strategy for Corrosion Minimization in Direct-Contact Lead-Bismuth/Water Systems
4. X. He, N. Li, M. Mineev, 2001, A kinetic model for corrosion and precipitation in non-isothermal LBE flow loop, *Journal of Nuclear Materials*, **297**, pp.214-219.
5. N. Li, V. Tcharnotskaria, T. Darling, C. Ammerman, X. He, J. King, D. Harkleroad, 2001, Lead-Bismuth Eutectic (LBE) Materials Test Loop (MTL) Test Plan, LA-UR-01-4866
6. N. Li, J. Zhang, 2003, Modeling Corrosion in Oxygen Controlled LBE Systems, *11th International Conference on Nuclear Engineering*, Tokyo, Japan, April 20-23, 2003.
7. J. Mizushima, H. Okamoto, H. Yamaguchi, 1996, Stability of flow in channel with a suddenly expanded part, *American Institute of Physics*, [S1070-6631(96)01710-2].
8. G. Schumacher, A. Heinzel, G. Müller, F. Zimmermann, Lead Alloys: Physico-Chemical Properties and Issues for their use in ADS Systems; The Control of Oxygen in Liquid Metal Systems.
9. V. Tcharnotskaria, C. Ammerman, T. Darling, J. King, N. Li, D. Shaw, L. Snodgrass, K. Woloshun, Liquid Lead-Bismuth Materials Test Loop, LAUR-01-5051
10. J. Zhang, N. Li, Parametric Study of a Corrosion Model Applied to Lead-Bismuth Flow Systems, *Journal of Nuclear Materials*, LA-UR-02-5416
11. A. Acrivos and M. Schrader, "Steady flow in a sudden expansion at high Reynolds numbers," Phys. Fluids 25, 923 (1982).
12. F. S. Milos and A. Acrivos, "Steady flow past sudden expansion at large Reynolds number – I. Boundary layer solution," Phys. Fluids 29, 1353 (1986).
13. F. S. Milos, A. Acrivos, and J. Kim, "Steady flow past sudden expansion at large Reynolds number – II. Navier-Stokes solution for the cascade expansion," Phys. Fluids 30, 7 (1987).
14. E. O. Macagno, and T. K. Hung, "Laminar eddies in a two dimensional conduit expansion," J. of Fluid Mech. 28, 43 (1967).
15. O. K. Kwon, R. H. Plether, and J. P. Lewis, "Prediction of sudden-expansion flows using the boundary-layer equations," J. Fluid Eng. 106, 285 (1984).
16. A. Kumar and K. S. Yajnik, "internal separated flows at large Reynolds numbers," J. Fluid mech. 97 27 (1980).
17. T. K. Hung, "Laminar flow in conduit expansions," Ph. D. dissertation, University of Iowa, Iowa City, 1966.
18. H. Morihara, "Numerical integration of the Navier-Stokes equations," Ph. D dissertation, State university of New York at Buffalo, 1972.
19. P. S. Scott, F. A. Mirza, and J. Vlachopoulos, "A finite element analysis of laminar flows through planar and axisymmetric abrupt expansions," Comput. Fluids 14,423 (1986).
20. M. Napolitano and P. Cinnela, "A numerical study of planar and axially-symmetric sudden expansion flows," Comput. Fluids 17, 185 (1989).
21. D. M. Hawken, P. Townsend, and M. F. Webster, "Numerical simulation of viscous flow in channels with a step," Comput. Fluids 20, 59 (1991).
22. A. Baloch, P. Townsend, and M. F. Webster, "On two- and three-dimensional expansion flows," Comput. Fluids 24, 863 (1995).
23. F. Durst, A. Melling, and J. H. Whitelaw, "Low Reynolds number flow over a plane symmetric sudden expansion," J. Fluid Mech. 64, 111 (1974).

24. W. Chedron, F. Durst, and J. H. Whitelaw, "Asymmetric flows and instabilities in symmetric ducts with sudden expansion," J. Fluid Mech. 84, 13 (1978).
25. R. M. Fearn, T. Mullin, and K. A. Cliffe, "Nonlinear flow phenomena in a symmetric sudden expansion," J. Fluid Mech. 211, 595 (1990).
26. M. Shapira, D. Degani, and D. Weihs, "Stability and existence of multiple solutions for viscous flow in suddenly enlarged channel," Comput. Fluids 18, 239 (1990).
27. D. Drikakis, "Bifurcation phenomena in incompressible sudden expansion flows," Phys. Fluids 9, 1 (1997).
28. X. He, N. Li and M. Mineev, "A kinetic model for corrosion and precipitation in non-isothermal LBE flow loop," Journal of Nuclear Materials 297 (2001) 214-219.
29. N. K. Ghaddar, K. Z. Korczak and B.B. Mikic, "Numerical investigation of incompressible flow in grooved channel. Part 1. Stability and self-sustained oscillations," J. Fluid Mech. 163, 99 (1986).
30. T. Y. Rizk, G. E. Thompson and J. L. Dawson, "Mass transfer enhancement associated with sudden flow expansion, " Corrosion Science, Vol. 38, No. 10, (1996).